

Interference Resurrection of the τ Dipole through Quantum Tomography

Prisco Lo Chiatto

*PRISMA⁺ Cluster of Excellence & Mainz Institute for Theoretical Physics
Johannes Gutenberg University, 55099 Mainz, Germany*

E-mail: plochiat@uni-mainz.de

ABSTRACT: Helicity selection rules can defy the expectation that the leading contributions from Standard Model Effective Field Theory operators occur at dimension 6, potentially reducing sensitivity to new physics scenarios. This paper investigates how spin correlations can restore ("resurrect") the interference contributions of the τ lepton's anomalous dipole moment. We first illustrate the mechanism for this interference restoration using a simple quantum mechanical example. We then calculate the sensitivity of these spin correlations to new physics. Additionally, we compute quantum information observables, namely measures of entanglement, Bell inequality violation, and the irreducible quantum uncertainty of the $\tau\tau$ state. Our findings show that spin correlation observables outperform both the cross-section and quantum information observables, by providing greater sensitivity to new physics and preserving information about CP violation.

Contents

1	Introduction	2
2	Interference Suppression and Resurrection in 4-Fermion Scattering	3
2.1	Resurrection in Spin Observables: a Quantum Mechanics Example	5
3	Spin Correlations and Quantum Tomography	7
3.1	Entanglement Measures and Inequalities	9
3.2	Tomography	11
3.3	Resurrection of the Dipole	13
3.4	Resurrection, Truncation and Unitarity	13
4	Case Study: τ-Dipoles at Colliders	15
4.1	Fano Coefficients	16
4.2	Quantum Observable and Spin Correlation	21
4.2.1	Lepton Colliders	21
4.2.2	SMEFT Sensitivity	23
4.2.3	Hadron Colliders	25
5	Conclusions and Outlook	26

1 Introduction

The search for deviations from the Standard Model (SM) has entered an era of precision tests. New physics (NP), whose characteristic scale Λ is well-separated from the electroweak (EW) scale v , can be described with the tools of effective field theory (EFT) to a largely model-independent extent. The Standard Model effective field theory (SMEFT) [1, 2] is one such EFT, which encodes the effect of heavy NP in a tower of operators, organised according to the number of derivatives and fields. In most cases, naive dimensional analysis (NDA) can be used to argue that the leading deviation from the SM prediction for a given observable is due to operators with canonical mass dimension 6. In particular, the leading deviation from the SM in observables is expected to arise at order $1/\Lambda^2$, corresponding to the interference between the SM matrix at dimension-6. However, (approximate) symmetries and selection rules can cause this expectation to fail [3–5]. In such cases, operators with higher mass dimension, loop corrections and multiple insertions of dimension 6 operators can have parametrically larger contributions than the interference. In Ref. [5], it was shown that a selection rule arises whenever the SM and SMEFT contribute to mutually exclusive helicity amplitudes. The chiral nature of the SM forces certain helicity amplitudes to vanish in the high-energy limit, generating emergent selection rules that are only lifted by finite masses.

In cases where noninterference happens, the sensitivity that a given observable has to NP effects is lowered by additional inverse powers of the large scale Λ . Noninterference can be circumvented by looking at different observables or different final states, in a process dubbed “interference resurrection.” For instance, if the final states are allowed to decay, the full process does not need to respect the helicity selection rule, and the interference is resurrected. One phenomenologically relevant case that has received much attention is triple gauge coupling, both for triple-W [6–8] and triple-gluon [9] case.

In this paper, we consider resurrection in 4-fermion scattering, which is relevant for searches at both lepton and hadron collider experiments. We show, through a quantum mechanical example, that the measurement of the spin correlations of final-state leptons in the process $f\bar{f} \rightarrow \ell\bar{\ell}$ can resurrect the interference of operators that electric and magnetic generate dipole moments, elucidating at the same time why the same procedure fails with other noninterfering operators. We therefore focus on the anomalous dipole moment of the τ , $g_\tau - 2$. Unlike the anomalous dipole moment of the lighter leptons, the short lifetime of the τ prevents $g_\tau - 2$ from being measured at low energies. Viable probes are then forced to be at high energies, and as such they suffer from noninterference, Spin correlation can then offer an interesting window on the anomalous dipole moments by resurrecting the interference.

Recently, the study of spin correlations at colliders has gained renewed interest, after the prediction [10] and successful measurement [11] of entanglement between the spin of a top quark pair at the Large Hadron Collider (LHC), as discussed in the review paper Ref. [12]. Following the formalism of the celebrated Bell inequalities [13], and of the groundbreaking experimental and theoretical efforts of the 1960s [14, 15], so-called “Bell tests” were developed. They aim to exclude hidden variable theories by measuring corre-

lations between spins that could not arise in theories based on local realism. At colliders, the correlation between the polarisation of the final states from hard scattering events are measured only indirectly. For unstable particles, the angular distribution decay product can be used instead, relying on angular momentum conservation.¹ This also explains, in part, why the measurement of spin correlations can resurrect the interference.

From a phenomenological and model building point of view, much of the recent effort on observables related to entanglement has been on establishing their sensitivity to physics beyond the Standard Model (BSM). For top quark pair production, it has been shown [18], that quantum information observables either surpass or complement the sensitivity of both the integrated cross-section and other angular observables. This seems to tie in perfectly with the fact that spin correlations can be used for interference resurrection, enhancing the sensitivity with respect to the cross-section. To test whether access to uniquely quantum phenomena is a necessary ingredient for increased sensitivity, we then evaluate the reach of different quantum information observables, and compare it to the spin correlation coefficient, which do not distinguish between classical and quantum correlations. We show that quantum information observables are suboptimal probes for 4-fermion operators, when compared with spin correlations, for instance because they partly erase the CP information. Indeed, we find that different choices for the phase of the Wilson coefficient lead to polarisation along different axes. The quantum information observables, combining all spin correlation in one measure, are unable to differentiate between different choices for the phase of the Wilson coefficients, causing the information about CP properties to be lost. We also evaluate the possible reach of present and future colliders.

The paper is structured as follows: in section 2, we introduce noninterference and resurrection of interference, then use a simple quantum mechanical example to explain the features of the resurrection mechanism. In section 3 we introduce the formalism to describe spin correlations, as well as the quantum information observables. In section 4 we calculate the spin observables for both lepton and hadron colliders, and critically analyse their NP reach. We conclude in section 5.

2 Interference Suppression and Resurrection in 4-Fermion Scattering

Heavy BSM physics generically impacts low energy observables through virtual corrections, which in the infrared are indistinguishable from higher dimensional operators; from this observation, coupled with the experimental fact that the symmetries of the SM seem to be a valid at low energy, one can organise BSM contributions in a largely model-independent way by considering all operators in an EFT built up from the SM fields in increasing mass dimension [1, 2]. We will adopt the SMEFT in this paper to discuss new physics effects, under the assumption that the underlying theory lives at a scale $\Lambda \gg v$.

In this paper, we will be interested in $f\bar{f} \rightarrow \ell\bar{\ell}$, with f a charged SM fermion and ℓ a charged SM lepton. At dimension 6 — the lowest dimension higher than 4 to affect this process at LO — the full list of SMEFT operator is well-known [1, 19]. Truncating

¹This measurement strategy is known to generate a loophole in Bell tests, see Refs. [16, 17]. Since the focus of this paper is not a test of quantum mechanics, this will not be an issue for us.

the operator basis at dimension 6, we can compute the squared matrix element, containing both SM and SMEFT contributions:

$$\mathcal{M} = \mathcal{M}^{\text{SM}} + \frac{1}{\Lambda^2} \mathcal{M}^{\text{SMEFT}}, \quad (2.1)$$

$$|\mathcal{M}|^2 = |\mathcal{M}^{\text{SM}}|^2 + 2\Re\left(\frac{1}{\Lambda^2} \mathcal{M}^{\text{SM}} \mathcal{M}^{\text{SMEFT}*}\right) + \frac{1}{\Lambda^4} |\mathcal{M}^{\text{SMEFT}}|^2, \quad (2.2)$$

$$\equiv |\mathcal{M}|^{2(0)} + \frac{1}{\Lambda^2} |\mathcal{M}|^{2(2)} + \frac{1}{\Lambda^4} |\mathcal{M}|^{2(4)}. \quad (2.3)$$

Using NDA, one can estimate the energy scaling for $|\mathcal{M}|^{2(n)}$. The interference contribution gives in most cases the leading deviation from the SM, simply because it carries fewer powers of the small ratio (E/Λ) than the SMEFT squared piece, where E is the energy scale of the hard interaction. However, as will be discussed shortly, selection rules can make the interference contribution vanish, rendering the SMEFT squared piece the leading deviation from the SM. In this case, the experimental sensitivity to this operator is expected to be much weaker than if the selection rule were absent, due to the energy suppression². Such a situation has been known since the 1990s to arise in the case of triple-gluon interaction [20, 21], as well as proposals to circumvent the suppression [9]. Recently, there has been renewed interest [3, 5, 22, 23], mostly for the phenomenologically important case of pair production of electroweak bosons; in this context, strategies to circumvent the helicity suppression go under the name of “interference resurrection” [24], that we will use throughout this paper.

Because the SM is a chiral theory, 4-fermion effective operators exhibit accidental selection rules in the limit of vanishing fermion masses, where helicity coincides with chirality. For instance, the three-point operators $f\bar{f}V$ ($V = \gamma, Z$), only allow f and \bar{f} to have opposite helicities, if the vector is transversely polarised. That is, the helicity matrix element $\mathcal{M}_{h_V h_f, h_{\bar{f}}}$, with h_X the helicity of particle X , satisfies

$$\mathcal{M}_{T--} = \mathcal{M}_{T++} = 0. \quad (2.4)$$

This implies specific helicity configurations for SM lepton pair production $f\bar{f} \rightarrow \ell\bar{\ell}$ mediated by electroweak gauge bosons at tree level. We will be interested in the cases $f = e, \mu, u, d, s$, all of which have small masses; since the coupling of fermions to longitudinally polarised gauge boson scales with the mass, we only need to consider transverse polarisation of the gauge boson. Then, the helicity matrix element $\mathcal{M}_{h_f h_{\bar{f}} h_\ell h_{\bar{\ell}}}$ is nonvanishing only when $h_f(h_\ell)$ is opposite to $h_{\bar{f}}(h_{\bar{\ell}})$. In the following, we will denote this by saying that the SM imposes the helicity structure $(h_f, h_{\bar{f}}, h_\ell, h_{\bar{\ell}}) = (+-+-), (-++-), (+--+), (-+-+)$. For nonzero lepton masses, the other helicity structures are suppressed by powers of $m_\ell/m_{\ell\ell}$, where $m_{\ell\ell}$ is the invariant mass of the di-lepton pair, and the longitudinal polarisation of the gauge bosons are likewise suppressed. In conclusion, in the SM:

$$\mathcal{M}_{h_f h_{\bar{f}} h_\ell h_{\bar{\ell}}}^{\text{SM}} = 0 + \mathcal{O}\left(\frac{m_\ell}{m_{\ell\ell}}\right) \quad \text{if } h_\ell = h_{\bar{\ell}} \text{ or } h_f = h_{\bar{f}}. \quad (2.5)$$

²Note that, if the dimension-6 squared contributions are considered, then the contributions of dimension-8 and loop-induced contributions can be of the same order and should generally to be considered when evaluating the sensitivity. This is beyond the scope of this paper.

Operator	Helicity Structure
$\bar{\ell}\gamma_\mu\ell A^\mu, \bar{\ell}\gamma_\mu\ell Z^\mu, \bar{\ell}\gamma_\mu\gamma^5\ell A^\mu, \bar{\ell}\gamma_\mu\gamma^5\ell Z^\mu$	$(+ - T), (- + T)$
$\mathcal{O}_{\ell\ell}, \mathcal{O}_{\ell edq}, \mathcal{O}_{\ell u}, \mathcal{O}_{\ell q}^1, \mathcal{O}_{\ell q}^3$	$(+ - + -), (- + + -), (+ - - +), (- + - +)$
$\mathcal{O}_{\ell equ}^1, \mathcal{O}_{\ell equ}^3$	$(+ + + +), (- - - -)$
$\mathcal{O}_{W\ell}, \mathcal{O}_{B\ell}$	$(+ + T), (- - T)$

Table 1. Operators that enter $\bar{f}f \rightarrow \bar{\ell}\ell$ up to dimension 6 in the SMEFT, and their helicity structure in the chiral limit. For the SMEFT operators we follow the notation of [19].

Given that SM leptons are light, at energies $m_{\ell\ell} \gtrsim 40$ GeV helicity-violating contributions are heavily suppressed even for the heaviest lepton, the τ . We refer to this as helicity suppression, and we call helicity selection rule the emerging selection rule in the exact chiral limit.

We now add dimension-6 SMEFT operators. Their helicity structures are summarised in table 1. Most operators that enter lepton pair production at dimension 6 in the SMEFT are unconstrained by helicity selection rules, as they have the same helicity structure as the SM. Only two classes of operators suffer from helicity suppression in the interference: the left-right quark-lepton 4-fermion operator $\mathcal{O}_{\ell equ}^1, \mathcal{O}_{\ell equ}^3$ and the dipole operators $\mathcal{O}_{W\ell}, \mathcal{O}_{B\ell}$. In both cases, in the chiral limit it is impossible to construct a non-zero interference $\mathcal{M}_{s_\ell s_{\bar{\ell}}}^{(SM)} \mathcal{M}_{s_\ell s_{\bar{\ell}}}^{(2)*}$, with $s_\ell(s_{\bar{\ell}}) = \pm 1$ the helicity of $\ell(\bar{\ell})$. We underline that in all contributions to the scattering of on-shell particles the same helicity structure is chosen for both matrix elements in the product, but as we will see this is not true for a generic observable. Indeed, the only way to resurrect interference is to find an observable that is built out of different helicity structures. In the next subsection, using a simple quantum mechanical example, we argue that spin observables can indeed display resurrection of interference.

2.1 Resurrection in Spin Observables: a Quantum Mechanics Example

Since leptons are a spin 1/2 particle, the spin state of a $\ell\bar{\ell}$ pair is represented by a bipartite two-qubit. That is, if we consider the initial state $|f\bar{f}\rangle$ to be a pure state, the final state can be expressed as:

$$|\psi\rangle = S|f\bar{f}\rangle = \sum_{s_\ell, s_{\bar{\ell}}} \mathcal{M}_{s_\ell s_{\bar{\ell}}} |s_\ell s_{\bar{\ell}}\rangle + \dots, \quad (2.6)$$

with S the scattering matrix, and the dots stand for all possible final states other than $\ell\bar{\ell}$. The spin state $|s_\ell s_{\bar{\ell}}\rangle$ is then, in general, not normalised, but contributes to $|\psi\rangle$ weighted by the S matrix element $\mathcal{M}_{s_\ell s_{\bar{\ell}}}$. Consider the simple case where $|\psi\rangle$ is the following pure, unnormalised state:

$$|\psi\rangle = a(|++\rangle + |--\rangle) + b(|+-\rangle - |-+\rangle), \quad (2.7)$$

where we have quantised the spins along the z axis. We recognise this state to be a linear combination of a triplet and singlet state. Given that these two states are orthogonal, they

do not interfere in the modulus squared of the final state:

$$\langle \psi | \psi \rangle = \sum_{s_\ell s_{\bar{\ell}}} |\mathcal{M}_{s_\ell s_{\bar{\ell}}}|^2 = |a|^2 + |b|^2. \quad (2.8)$$

We can consider also spin observables by insertion of the spin operators $S_i^\ell = \sigma_i \otimes \mathbb{1}_2$, $S_i^{\bar{\ell}} = \mathbb{1}_2 \otimes \sigma_i$, with σ the Pauli matrices. The correlation between the two spins, both measured along the z axis, is given by

$$\langle \psi | S_z^\ell S_z^{\bar{\ell}} | \psi \rangle = |a|^2 - |b|^2, \quad (2.9)$$

which, like the modulus squared, only depends on the two coefficients squared, so it receives no contributions from interference. It would be too hasty to conclude at this point that the orthogonality of the two states prevents them from interfering in all observables. Indeed, interference generates the polarisation of ℓ along the y axis, because the S_y^ℓ operator causes a spin flip:

$$\begin{aligned} \langle \psi | S_y^\ell | \psi \rangle &= \langle \psi | (a(|-+\rangle - |+-\rangle) + b(|--\rangle + |++\rangle)) \\ &= 4\Im(ab^*). \end{aligned} \quad (2.10)$$

And similarly we find a nonzero interference when considering the expectation value of $S_z^\ell S_x^{\bar{\ell}}$, which gives the correlation between the two spins, when measured along the z and x axis, respectively:

$$\langle \psi | S_z^\ell S_x^{\bar{\ell}} | \psi \rangle = -2\Re(ab^*). \quad (2.11)$$

Measuring the full set of spin observables, as well as the modulus square, can then be used to fully reconstruct $|\psi\rangle$. In contrast, a measurement of the probability cannot access the relative phase between a and b . This is the essence of a process called “quantum tomography” [25]; we discuss quantum tomography at colliders in section 3.2.

Let us now add the effect of classical uncertainty, to describe polarisation and other degrees of freedom. This is best done using a density matrix. We recall that for a given state $|\psi\rangle$, which is represented by a statistical ensemble of pure states $|\phi_i\rangle$, the density matrix ρ is expressed by the weighted sum of the projectors over $|\phi_i\rangle$:

$$\rho = |\psi\rangle \langle \psi| = \sum_i p_i |\phi_i\rangle \langle \phi_i|, \quad (2.12)$$

where $\{|\phi_i\rangle\}_i$ is a basis for the Hilbert space of the system, and the p_i sum to one. In the present case of a bipartite qubit, ρ will be a $2^2 = 4$ -dimensional square matrix.

We will assume the initial state is an unpolarised beam, represented as an equiprobable ensemble ρ_i :

$$\rho_i = 1/4 \begin{pmatrix} 1 & 0 & 0 & 0 \\ 0 & 1 & 0 & 0 \\ 0 & 0 & 1 & 0 \\ 0 & 0 & 0 & 1 \end{pmatrix}. \quad (2.13)$$

We will have the scattering matrix S act on the pure states as:

$$\begin{cases} |++\rangle \rightarrow \sqrt{2}a|++\rangle \\ |--\rangle \rightarrow \sqrt{2}a|--\rangle \\ |+-\rangle \rightarrow b(|+-\rangle + |-+\rangle) + c(|++\rangle + |--\rangle) \\ |-+\rangle \rightarrow b(|+-\rangle + |-+\rangle) + c(|++\rangle + |--\rangle) \end{cases}, \quad (2.14)$$

that is, in matrix form

$$S = \begin{pmatrix} \sqrt{2}a & 0 & 0 & 0 \\ c & b & b & c \\ c & b & b & c \\ 0 & 0 & 0 & \sqrt{2}a \end{pmatrix}. \quad (2.15)$$

The action of S was chosen to mimic the 4-fermion interaction we study in this paper. In particular, the action on the equal-sign states (a channel) mimics the $\mathcal{O}_{\ell equ}^1, \mathcal{O}_{\ell equ}^3$ operators, while the action on the mixed-sign states (b and c channels) mimics the SM and the dipole operators, respectively.

-he trace of the final state, which computes the weighted average of all the pure states square modulus is

$$A = \text{Tr}(S\rho_i S^\dagger) = |a|^2 + |b|^2 + |c|^2, \quad (2.16)$$

which does not receive contributions from interference. On the other hand, the correlation matrix of the two spins along the three axes is given by

$$\tilde{C} = \text{Tr}(\vec{S}^\ell \otimes \vec{S}^{\bar{\ell}} S\rho_i S^\dagger) = \begin{pmatrix} |b|^2 + |c|^2 & 0 & 0 \\ 0 & |b|^2 - |c|^2 & 2\Im(bc^*) \\ 0 & 2\Im(bc^*) & |a|^2 - |b|^2 + |c|^2 \end{pmatrix}, \quad (2.17)$$

which shows interference between the b and c channels in the (yz) and (zy) components. The a channel, on the other hand, does not interfere with the other two channels because the initial states are in a classical admixture. If the a channel had a nonzero action on the mixed-sign spin configurations, it would interfere with the b channel, even though it induces an orthogonal spin configuration in the final state. The simple examples in this subsection demonstrate how interference can be resurrected in spin correlations: The interference between orthogonal final states is generated by a spin-flip operator, but only if the states are in a quantum superposition.

We now introduce the necessary formalism for describing quantum tomography measurements at a collider experiment.

3 Spin Correlations and Quantum Tomography

We study spin correlations in 4-fermion scattering $f\bar{f} \rightarrow \ell\bar{\ell}$. As argued before, the final state $|\ell\bar{\ell}\rangle$ can be expressed in terms of a 4×4 density matrix, called the spin-density matrix,

defined using the S -matrix elements as follows [26]:

$$R_{s_{\ell,1}s_{\ell,2},s_{\bar{\ell},1}s_{\bar{\ell},2}}^I \equiv \frac{1}{N^2} \sum_{f,\bar{f} \text{ d.o.f.}} \mathcal{M}_{s_{\ell,2}s_{\bar{\ell},2}}^* \mathcal{M}_{s_{\ell,1}s_{\bar{\ell},1}}, \quad (3.1)$$

$$\mathcal{M}_{s_{\ell}s_{\bar{\ell}}} \equiv \langle \ell(k_1, s_{\ell}) \bar{\ell}(k_2, s_{\bar{\ell}}) | S | f(p_1) \bar{f}(p_2) \rangle, \quad (3.2)$$

where $\mathcal{M}_{s_{\ell}s_{\bar{\ell}}}$ are the polarised scattering matrix elements with s_{ℓ} ($s_{\bar{\ell}}$) the ℓ (anti- ℓ) spin, taking values $+$, $-$.

We average over discrete degrees of freedom (d.o.f.), such as spin and color, by summing incoherently over them and dividing by an appropriate normalisation factor N for each initial state fermion. The sum is incoherent because we assume the initial state is a mixed state with uniform statistical distribution over the initial d.o.f. (i.e. we assume unpolarised beams). This results in the final state being mixed [26]. In contrast, the final state spin d.o.f. are in a quantum superposition. Note also that while we defined R to have four indices, the indices $(s_{\ell,1}s_{\bar{\ell},1})$ and $(s_{\ell,2}s_{\bar{\ell},2})$ can be combined to make R a 4×4 matrix.

Any 4×4 matrix can be decomposed in terms of products of Pauli matrices σ^i in terms of so-called Fano coefficients as follows [27]:

$$R = A \mathbb{1}_4 + \tilde{B}_i^+ \sigma^i \otimes \mathbb{1}_2 + \tilde{B}_i^- \mathbb{1}_2 \otimes \sigma^i + \tilde{C}_{ij} \sigma^i \otimes \sigma^j, \quad (3.3)$$

where we can recognise the spin operator acting on a single particle, $S_i^- = \mathbb{1}_2 \otimes \sigma_i$, $S_i^+ = \mathbb{1}_2 \otimes \sigma_i$, as well as their product, $S_i^- S_j^+ = \sigma_i \otimes \sigma_j$. Indeed, A is the overall normalisation of R , the vector \tilde{B}_i^+ (\tilde{B}_i^-) quantifies the spin polarisation of the (anti-)particle, while the matrix \tilde{C}_{ij} contains the correlation between the spin of the two particles. The probability of a given spin configuration $(s_{\ell}, s_{\bar{\ell}})$ being measured is

$$P(s_{\ell}, s_{\bar{\ell}}) = \frac{1}{N^2} \sum_{f,\bar{f} \text{ d.o.f.}} |\mathcal{M}_{s_{\ell}s_{\bar{\ell}}}|^2. \quad (3.4)$$

A is the trace of R , that is the sum of all the probabilities. This is, of course, proportional to the differential cross section:

$$\frac{d\sigma}{d\Omega} = \frac{\alpha^2 \beta_{\ell}}{m_{\ell\bar{\ell}}^2} A(m_{\ell\bar{\ell}}, \mathbf{k}), \quad (3.5)$$

where $m_{\ell\bar{\ell}}^2 = (p_{\ell} + p_{\bar{\ell}})^2$ is the di-lepton invariant mass squared, α an appropriate coupling constant, $\beta_{\ell} = \sqrt{1 - 4m_{\ell}^2/m_{\ell\bar{\ell}}^2}$ is the ℓ velocity and Ω the solid angle defined by the direction \mathbf{k} . On the other hand, the probability of the spin measurement on ℓ having the outcome (s_{ℓ}) can be obtained from the reduced density matrix, defined by tracing out the $\bar{\ell}$ spin d.o.f.:

$$\text{Tr}_{\bar{\ell}}(R)_{s_{\ell}s'_{\ell}} = \sum_{s_{\bar{\ell}}} \mathcal{M}_{s'_{\ell}s_{\bar{\ell}}}^* \mathcal{M}_{s_{\ell}s_{\bar{\ell}}} \quad (3.6)$$

$$P(s_{\ell}) = \frac{1}{N^2} \sum_{f,\bar{f} \text{ d.o.f.}} \left| \sum_{s_{\bar{\ell}}} \mathcal{M}_{s_{\ell}s_{\bar{\ell}}} \right|^2 = \sum_{s_{\bar{\ell}}} P(s_{\ell}, s_{\bar{\ell}}) + 2(\mathcal{M}_{s_{\ell},-} \mathcal{M}_{s_{\ell},+}^*). \quad (3.7)$$

As we saw in the previous subsection, the probabilities of the spin measurements on a single particle, and thus also their correlations, depend not only on the matrix element squared, but also on the interference between matrix elements with different spin structures. Differently, the initial d.o.f. are in a classical admixture and do not interfere quantum mechanically.

At this point, one can normalise the spin-density matrix as $\rho = R/\text{Tr}[R]$ to obtain a density matrix. We can now expand ρ in the same form as the spin-production matrix (note the absence of tildes)

$$\rho = \frac{1}{4}(\mathbb{1}_4 + B_i^+ \sigma^i \otimes \mathbb{1}_2 + B_i^- \mathbb{1}_2 \otimes \sigma^i + C_{ij} \sigma^i \otimes \sigma^j). \quad (3.8)$$

If the initial state is composite, like at a pp collider, the full density matrix can be factorised as a classical ensemble of the individual partonic contributions, weighted by the luminosity function I_q [10]:

$$\rho_{ijkl}^{pp} = \frac{\sum_q I_q R_{ijkl}^{qq}}{\sum_q I_q A^{qq}}. \quad (3.9)$$

The luminosity functions are defined as:

$$I_{qq}(\hat{m}) = \frac{2\hat{m}}{\sqrt{s}} \int_{\hat{m}}^{1/\hat{m}} \frac{dz}{z} q_q(\hat{m}z) q_{\bar{q}}\left(\frac{\hat{m}}{z}\right), \quad (3.10)$$

with $\hat{m} = m_{\ell\bar{\ell}}/\sqrt{s}$, and $q_q(x)$ is the PDF of the parton q . The numerical value of the PDFs are taken from the PDF4LHC collaboration [28] and evaluated with the help of the Mathematica interface ManeParse [29]. We will consider only $q = u, d, s$ because the luminosity functions of heavier quarks are negligibly small.

Finally, we will be interested in the density matrix integrated over the solid angle $d\Omega = \sin\theta d\theta d\phi \equiv dz d\phi$, with Ω the scattering angle of the hard scattering, so we define an integrated spin-production matrix and density matrix:

$$\begin{aligned} R^{\text{Integrated}} &= \frac{1}{4\pi} \int dz d\phi R, \\ \rho^{\text{Integrated}} &= \frac{R^{\text{Integrated}}}{A^{\text{Integrated}}}. \end{aligned} \quad (3.11)$$

Having defined the necessary density matrix, we consider how to define the amount of entanglement it contains.

3.1 Entanglement Measures and Inequalities

A density matrix represents an entangled state if and only if its density matrix can be expressed as a convex combination of product states, i.e.

$$\rho = \sum_{ij} p_{ij} \rho_i^+ \otimes \rho_j^-, \quad (3.12)$$

where ρ_i^\pm is a one-qubit state density matrix on the Hilbert space of the (anti-)particle and the real-valued p_{ij} are non-negative and sum to one. If such a decomposition does

not exist, the state is said to be entangled [30], because knowledge about the Hilbert space of each single subsystems does not translate to knowledge about the full Hilbert space, a purely quantum phenomenon. This formal definition does not provide however a quantitative handle on the entanglement; moreover explicitly checking whether a state is separable involves proving a negative, a generically hard task. For these reasons various quantities have been devised to measure entanglement (see e.g. [31] for a review). The specific case of two-qubit bipartite states is the best-understood one, and a plethora of so-called “entanglement witnesses” with explicit analytic expressions are available. To be an entanglement witness, a measure of entanglement must attain its minimum value (usually zero) for pure states and its maximum value at maximally entangled states (such as Bell pairs).

Concurrence One entanglement witness that is often used is the concurrence $\mathcal{C}[\rho]$ [32], defined in terms of the spin-flipped density matrix $\tilde{\rho} = (\sigma_2 \otimes \sigma_2)\rho^*(\sigma_2 \otimes \sigma_2)$. The decreasingly ordered eigenvalues λ_i of the matrix $\omega = \sqrt{\sqrt{\rho}\tilde{\rho}\sqrt{\rho}}$ or, equivalently, the square root of the eigenvalues of the matrix $\Omega = \rho\tilde{\rho}$, are used to define [32]

$$\mathcal{C}[\rho] = \max(0, \lambda_1 - \lambda_2 - \lambda_3 - \lambda_4). \quad (3.13)$$

Null concurrence is attained for separable states, while the maximum value of 1 is attained for maximally entangled states.

CHSH Inequality Arguably the most famous form of non-classical correlations is the violation of so-called Bell inequalities, which are always satisfied in local and realistic theories. A particularly useful form, the CHSH (Clauser-Horne-Shimony-Holt) inequality [15], allowed the first-ever experimental determination of Bell non-locality [14] and is still a cornerstone of quantum information studies.

For two-qubit systems, the so-called “Horodecki criterion” for violating the CHSH inequality can be calculated in terms of the spin correlation matrix C only [33]. One defines (m_1, m_2, m_3) as the eigenvalues of $M = C^T C$ in decreasing order. According to the Horodecki criterion, the CHSH inequality is violated if and only if [33]

$$\mathbf{m}_{12} = m_1 + m_2 > 1. \quad (3.14)$$

Maximum violation is obtained at $\mathbf{m}_{12} = 2$, and separable states have $\mathbf{m}_{12} = 0$. It is worth noting that, in general, violation of Bell inequalities is a stronger condition than entanglement; the two notions coincide only for pure two-qubit bipartite states [34].

Simplified Criteria It is clear that, if the polarisation vectors B^\pm are vanishing, all the information about entanglement is contained in the correlation matrix C . This happens if the individual leptons are not produced in a polarised state by the interaction due to, for example, separate conservation of C and P parities [35]. In that case, the C matrix elements are also constrained, and indeed the correlation matrix is block-diagonal [10]. Sufficient (but not necessary) conditions for Bell inequality violation and entanglement can be obtained from the Peres-Horodecki criterion [36] with reference only to the diagonal

elements of the C matrix. We will not pursue this direction, because as we show in section 2.1, resurrection of interference is active only in the off-diagonal elements of the C matrix. Moreover, EW interactions violate both P and C parities.

Quantum Discord It has long been recognised [37] that there exist separable mixed states whose correlation cannot be described by a classical theory, which has prompted the search for finer discriminant between classical and quantum states, see Ref. [38] for a recent review. Various measures have been devised, focusing on different aspects of quantum mechanics, such as the fact that a local measurement on subsystems can induce disturbances in the overall system. Most of the measures of quantum correlations are called “discord”, because they measure the difference between two generalisations of spin correlations that would coincide in the classical case. Many of the measures of discord involve complicated minimisation processes and are hence not easily amenable to calculations, without employing simplifying assumptions on the nature of the state, as for example can be done in top pair production [39].

In this work we will focus on one definition of quantum correlations that has a relatively simple expression, the Local Quantum Uncertainty (LQU) [40]. It quantifies the irreducible quantum uncertainty in local measurements on a subsystem. The LQU is zero if and only if there exists at least one observable that can be measured on a subsystem that is not affected by quantum uncertainty. The LQU is defined as [40]

$$LQU(\rho) = 1 - \max(\text{Eig}(W)), \quad (3.15)$$

$$W_{ij} = \text{Tr}(\sqrt{\rho}(\sigma_i \otimes \mathbb{1}_2)\sqrt{\rho}(\sigma_j \otimes \mathbb{1}_2)). \quad (3.16)$$

We now consider how to experimentally measure spin polarisations and correlations.

3.2 Tomography

Collider experiments are generically not able to directly measure the spin of outgoing particles. Luckily, due to angular momentum conservation, the spin information of a decaying particle is imprinted in its decay products. By selecting one of the decay products $d^+(d^-)$ for the outgoing lepton (antilepton), we can relate the spin density matrix to the doubly-differential distribution in the decay product angles [41]. In particular, in the narrow-width approximation one obtains [26]

$$\frac{d\sigma}{d\cos\theta_{\pm}^i} \propto 1 \pm B_i^{\pm} \cos\theta_{\pm}^i, \quad (3.17)$$

$$\frac{d^2\sigma}{d\cos\theta_+^i d\cos\theta_-^j} \propto 1 + C_{ij} \cos\theta_+^i \cos\theta_-^j \ln \cos\theta_+^i \cos\theta_-^j, \quad (3.18)$$

where we define the polar angle with respect to a given direction \hat{u}_i through $\cos(\theta_{\pm}^i)^i \equiv \hat{d}^{\pm} \cdot \hat{u}_i$, with $\hat{d}^+(\hat{d}^-)$ the direction of flight of the decay product we picked for the lepton (antilepton). This is the basis of *quantum tomography*: from repeated measurement of angular correlations, one can reconstruct the density matrix, hence the state, of the outgoing $\ell\bar{\ell}$ pair. We note that many different ways have been devised to reconstruct the C matrix,

by using different definitions of the notion of correlation, but they all perform similarly in terms of experimental uncertainties [42, 43].

We compute the density matrix in the helicity basis $\{\hat{r}, \hat{n}, \hat{k}\}$, where \hat{k} points along the $\bar{\ell}$ 3-momentum and the other two unit vector are defined with reference to a fourth unit vector \hat{p} :

$$\hat{p} \cdot \hat{k} = z, \quad (3.19)$$

$$\hat{r} = \frac{1}{\sqrt{1-z^2}}(\hat{p} - z\hat{k}), \quad (3.20)$$

$$\hat{n} = \frac{1}{\sqrt{1-z^2}}\hat{k} \times \hat{p}. \quad (3.21)$$

The helicity basis is event-dependent, thus the state that one reconstructs is in general not a proper quantum state but a so-called fictitious state [26]. Nonetheless, fictitious states retain the information of the single measurements that were used for its reconstruction, even though this information might get smeared [44].

We should note at this point that measuring the angular correlations of the decay products of ℓ requires a reconstruction of the momentum of ℓ , as well of the c.o.m. frame. At lepton colliders, the center of mass is known with precision, and possible invisible particles in the decay products can be reconstructed using impact parameters [45]. The situation is more complicated at hadron colliders, where the composite nature of the hadron makes the c.o.m. frame of the hard scattering *a priori* unknown. We will revisit this issue later.

Based on the discussion in this section, we want to highlight a conceptual difference between the existing descriptions of interference resurrection in the literature and the mechanism presented in section 2.1. In diboson production, interference resurrection has been studied extensively, both in the triple-W [6–8] and triple-gluon [9] contexts. It has been noted that the operator \mathcal{O}_{3V} does not interfere with the Standard Model (SM) in the process $f\bar{f} \rightarrow VV$ [20, 21], but interference is restored by considering a larger process where $f\bar{f} \rightarrow VV$ is an intermediate stage, VV being off-shell[9, 22, 23].³ It has also been observed that interference can be artificially canceled if a strict narrow-width approximation is used [6], making a correct quantum treatment of the intermediate VV state crucial. As reviewed, measuring spin polarization typically requires the decay of the final-state particle. However, our discussion in section 2.1 clarifies that the key factor is not decay or the particle being off-shell, but a proper quantum mechanical treatment. Thus, even if we had direct access to the spins of (on-shell) particles at colliders, quantum mechanics would still govern the resurrection phenomenon, independent of the specific spin measurement procedures

Having defined the observables needed for the measurement of spin observables, we turn now to their calculation, and to the question of whether they can display resurrection of interference. First, we categorise the SM and SMEFT contributions to $f\bar{f} \rightarrow \ell\bar{\ell}$.

³In density matrix terminology, Ref.[46] discusses resurrection in electroweak boson production.

3.3 Resurrection of the Dipole

We are now ready to discuss the resurrection of dimension-6 operators in 4-fermion scattering. As we noted before, only the left-right operators $\mathcal{O}_{\ell equ}^1, \mathcal{O}_{\ell equ}^3$ and the dipole operators $\mathcal{O}^{\ell V}$ exhibit different helicities structure than the SM. It is clear from the discussion in section 2.1 that the contact operators do not interfere with the SM at all, even in the off-diagonal elements of the R matrix, because we sum over (fixed) initial fermion polarisation a, b . So we will not consider them going forward.

We turn now to the dipole operator class. As we just argued, modifying the helicity selection rules for the initial states makes the interference impossible; therefore we focus on final-state dipole operator $\mathcal{O}_{\ell V}$. Note that the gauge boson is fixed to be transverse by the vanishing mass of initial fermions, regardless of any helicity selection rules involving the final leptons. The dipole operator imposes the $(T + +), (T - -)$ configuration in the chiral limit, which means that the full process $f\bar{f} \rightarrow V \rightarrow \ell\bar{\ell}$ will have the $(+ - ++), (+ - --), (- + ++), (- + --)$ structure in the chiral limit:

$$\mathcal{M}_{s_\ell s_{\bar{\ell}}}^{\text{Dipole}} = 0 + \mathcal{O}\left(\frac{m_\ell}{m_{ll}}\right) \quad \text{if } s_\ell \neq s_{\bar{\ell}}. \quad (3.22)$$

Unlike the contact operators, then, the dipole operator interference with the SM populates the off-diagonal entries of the R matrix. The leptonic dipole operators are unique since they are the only class of operators suffering from helicity suppression in the interference, but still contributing an interference term to spin correlations.

We now explore the NP reach and resurrection properties of spin correlation, both quantum and not.

3.4 Resurrection, Truncation and Unitarity

Before proceeding, it is important to address a subtlety related to the mismatch in large-energy behaviour of the various entries of the R matrix, which arises due to the non-interference and resurrection phenomena: the R matrix, truncated at order Λ^2 , violates perturbative unitarity at energies lower than the cutoff. To clarify, let us separate the various contributions to a given observable based on their Λ dependence and energy scaling from naive dimensional analysis (NDA). The dipole operator has the NDA scaling of $vm_{\ell\ell}/\Lambda^2$ for interference contributions. However, due to the helicity selection rule only the SMEFT squared scales with energy, while the interference is proportional to the constant chirality-flip factor vm_ℓ/Λ^2 [47]:

$$\frac{d\sigma}{d\Omega} \Big|_{m_{\ell\ell} \gg m_\ell} \xrightarrow{\text{}} \frac{d\sigma^{(0)}}{d\Omega} + \frac{vm_\ell}{\Lambda^2} \frac{d\sigma^{(2)}}{d\Omega} + \frac{v^2 m_{\ell\ell}^2}{\Lambda^4} \frac{d\sigma^{(4)}}{d\Omega}, \quad (3.23)$$

and similarly we can define $A^{(n)}$ and $R^{(n)}$ by looking at the high-energy behaviour. This means that A receives a small, energy-independent contribution at order Λ^2 . However, due to resurrection, the off-diagonal entries of the R matrix, at order Λ^2 , have the NDA scaling

of $m_{\ell\ell}$ at large energies:

$$\begin{aligned} R_{ii} &\xrightarrow{m_{\ell\ell} \gg m_\ell} R_{ii}^{(0)} + \frac{vm_\ell}{\Lambda^2} R_{ii}^{(2)} + \frac{v^2 m_{\ell\ell}^2}{\Lambda^4} R_{ii}^{(4)}, \\ R_{ij} &\xrightarrow{m_{\ell\ell} \gg m_\ell} R_{ij}^{(0)} + \frac{vm_{\ell\ell}}{\Lambda^2} R_{ij}^{(2)} + \frac{v^2 m_{\ell\ell}^2}{\Lambda^4} R_{ij}^{(4)}, \quad i \neq j. \end{aligned} \quad (3.24)$$

Therefore, if we neglected the SMEFT squared contributions, the off-diagonal terms of the normalised density matrix would also grow like $m_{\ell\ell}$ at large energies:

$$\rho_{ij} = \frac{R_{ij}^{(0)} + \frac{vm_{\ell\ell}}{\Lambda^2} R_{ij}^{(2)}}{A^{(0)} + \frac{vm_\ell}{\Lambda^2} A^{(2)}} \xrightarrow{m_{\ell\ell} \gg m_\ell} \frac{R_{ij}^{(0)} + \frac{vm_{\ell\ell}}{\Lambda^2} R_{ij}^{(2)}}{A^{(0)}} \quad i \neq j. \quad (3.25)$$

If we instead include the order Λ^4 contributions, both the diagonal and off-diagonal entries of R grow like $m_{\ell\ell}^2$ at large energies. Then, the energy dependence asymptotically cancels and the ρ matrix elements approach constant values at large energies.

Truncating at order Λ^2 would result in a violation of perturbative unitarity in the ρ matrix, at energies lower than the nominal cutoff scale Λ . Such a truncation is, however, clearly not permitted, because the SMEFT squared contribution dominates over the interference. Consequently, this affects the entanglement witnesses, causing them to grow over their theoretical maximum of 2 for \mathbf{m}_{12} and 1 for $\mathcal{C}[\rho]$.⁴ We emphasise that such a violation of perturbative unitarity happens at energies lower than Λ , and as such does not seem directly related to possible violation of unitarity at or past the cutoff; moreover the full R matrix up to order Λ^2 does not exhibit violation of perturbative unitarity at any energy, even past the cutoff.

In order to avoid spurious violations of unitarity while still being able to observe the effect of resurrection of the interference, we define $\rho^{\text{No Int}}$ by ignoring the interference terms:

$$\rho^{\text{No Int}} = \frac{R^{(0)} + \left(\frac{vm_{\ell\ell}}{\Lambda^2}\right)^2 R^{(4)}}{A^{(0)} + \left(\frac{vm_{\ell\ell}}{\Lambda^2}\right)^2 A^{(4)}}. \quad (3.26)$$

Another option would be to normalise by the full cross-section A . While at large energies the two choices differ negligibly, at low energies the density matrix would not be properly normalised; thus we find the definition in eq. (3.26) more appropriate.

In the absence of resurrection, the difference between $\rho^{\text{No Int}}$ and the full spin density matrix is proportional to the small, energy-independent ratio vm_ℓ/Λ^2 . On the other hand, resurrection of interference causes the difference between ρ and $\rho^{\text{No Int}}$ to grow linearly with energy. A successful resurrection should also improve the sensitivity at moderate and low energies.

We now turn to observables that quantise entanglement and other quantum information concept.

⁴The sensitivity of quantum information observables to unitarity violations has been explored in [46] for longitudinal boson scattering.

4 Case Study: τ -Dipoles at Colliders

Having motivated the choice for the class of dipole operators, we will specialise to τ leptons. The motivation is twofold: first, flavour-universal BSM models, as well as loop effects in the SM, give rise to larger contributions to the τ dipole than to the other lighter fermions [48].⁵ Second, unlike the electron and muon $g - 2$, which have been measured to incredible precision [54, 55], direct low-energy measurements of $g_\tau - 2$ are precluded by the tiny lifetime of the τ . Current and prospective sensitivity to tau dipoles comes from high-energy collisions: a direct measurement at a fixed-target experiment has been proposed [56, 57], while indirect bounds are extracted from collider experiments such as B -factories [58–63], electron-electron [64, 65], proton-proton [47, 66], or ion-ion [67–69] collisions, by constraining the anomalous τ -lepton coupling to off-shell photons or detecting a radiation zero in radiative τ decays [70, 71]. All these probes suffer from non-interference and, partly as a result, the current sensitivity is orders of magnitude above the precise SM prediction [72]. Moreover the sign and phase of the Wilson coefficients remain unconstrained.

Therefore, in this work we will consider the following lagrangian:

$$\mathcal{L} = \mathcal{L}_{\text{SM}} + \mathcal{L}_{\text{SMEFT}} , \quad (4.1)$$

$$\mathcal{L}_{\text{SM}} = e Q_\ell A_\mu \bar{\ell} \gamma^\mu \ell + \frac{e}{s_W c_W} (Z_\mu \bar{\ell} \gamma^\mu (Q_{V\ell} + Q_{A\ell} \gamma^5) \ell) , \quad (4.2)$$

$$\mathcal{L}_{\text{SMEFT}} = \frac{c_{\tau B}}{\Lambda^2} (\bar{L}_L \sigma^{\mu\nu} \tau_R) H B_{\mu\nu} + \frac{c_{\tau W}}{\Lambda^2} (\bar{L}_L \sigma^{\mu\nu} \sigma_3 \tau_R) H W_{\mu\nu}^3 + \text{h.c.} , \quad (4.3)$$

where $L_L = (\nu_{\tau L}, \tau_L)^T$ is the left-handed third-generation lepton doublet, τ_R is the right-handed third generation weak singlet, H is the Higgs boson, and $B^{\mu\nu}$ and $W_{\mu\nu}^3$ stand for the $U(1)_Y$ and the neutral $SU(2)_L$ field-strength tensors, respectively. After electroweak-symmetry breaking, we can rotate the effective couplings by the weak mixing angle,

$$c_\gamma = \cos \theta_W c_{\tau B} - \sin \theta_W c_{\tau W} , \quad (4.4)$$

$$c_Z = \sin \theta_W c_{\tau B} + \cos \theta_W c_{\tau W} . \quad (4.5)$$

We further set the Higgs field to its vacuum expectation value v , which renders the dimension-6 operator a three-point interaction. The rotated couplings in eq. (4.5) then correspond to the τ -lepton dipole interactions with the photon and the Z -boson. Neglecting higher-order corrections, it is possible to relate the effective coupling c_γ to contributions to the anomalous magnetic and electric moments of the τ -lepton,

$$\Delta a_\tau = \frac{2\sqrt{2}}{e} \frac{m_\tau v}{\Lambda^2} \Re(c_\gamma) + \dots , \quad (4.6)$$

$$\Delta d_\tau = -\sqrt{2} \frac{v}{\Lambda^2} \Im(c_\gamma) + \dots , \quad (4.7)$$

⁵Such enhancements can be even larger in scenarios with new bosons coupled to both lepton chiralities, yielding contributions to dipoles $\propto m_\ell m_F / \Lambda^2$, where m_F denotes the mass of the heavy fermion running in the loops [49]. Examples are leptoquark models [50], where F is a heavy quark such as the bottom-quark [51, 52], or scenarios where F can be a heavy vector-like lepton [53].

where the dots stand for loop corrections, cf. Ref. [49, 73], and similarly weak magnetic and electric moments can be defined. We will also find it useful to define $C_{\gamma(Z)} = c_{\gamma(Z)}/\Lambda^2$.

In the rest of this section we present our results. We analytically calculate the R -matrix in the EW SM at tree level, as well as with the addition of the SMEFT dipole operators $\mathcal{O}_{\gamma\tau}, \mathcal{O}_{Z\tau}$ with the help of FeynArts and FormCalc [74, 75]. We collect the coefficient of the resulting Fano decomposition in section 4.1.

After integrating over z , we calculate, as a function of $m_{\tau\tau}$, the Bell inequality marker \mathfrak{m}_{12} , the concurrence $\mathcal{C}[\rho]$, and the local quantum uncertainty LQU. We pick as a benchmark point the current best constraint $|C_\gamma| \leq (1.5 \text{ TeV})^{-2}$ [47] and, since our goal is to compare the reach of different observables to NP, we apply it to $|C_Z|$ as well. We consider 4 possible phases for the Wilson coefficient, to showcase the sensitivity of different observables to the phase of the Wilson coefficients.

Finally, we compare the quantum information observables to single elements of the C matrix, and show how the latter have better sensitivity both at high and low energies to the SMEFT operators, as well as better discrimination power between different phase choices for the Wilson coefficient, hence to the CP properties of the UV theory. We perform this procedure both for ee and pp colliders.

4.1 Fano Coefficients

Explicit expression for the R matrix in the electroweak SM, as well as with a parametrisation of the effect of anomalous dipole contributions, first appeared in [76], but they were not calculated in the helicity basis that we adopt here. The Fano coefficients for $f\bar{f} \rightarrow \ell\bar{\ell}$ in the EW theory, calculated in the helicity basis, have first appeared in [18]; we agree with their results on most terms, but we find some non-vanishing off-diagonal correlation that were not considered in [18]. These terms are due to the non-zero Z width, and they generate absorptive contributions to the matrix elements, which cannot be generated from the $\Gamma_Z = 0$ expression by the usual substitution $m_Z^2 \rightarrow m_Z^2 - im_Z\Gamma_Z$. Of course, contributions linear in Γ_Z are formally one loop and small in the SM due to the small ratio Γ_Z/M_Z , but nonetheless they modify the spin configuration of the final state, and might be relevant for other vector mediators with larger widths. Moreover, we explicitly write down the polarisation vector B , which has not appeared elsewhere.

Following [18] we divide the contributions according to their tensor structure, that is we split the spin production matrix in three parts:

$$R = R^{[0]} + R^{[1]} + R^{[2]}, \quad (4.8)$$

where the superscript indicates the number of γ^5 insertions on the τ line. This is because the tensor structure uniquely defines the spin state. Moreover, still following [18], we denote common factors by F . Throughout this section, the coefficient that are not explicitly written are either zero or can be obtained by the known symmetry of the Fano coefficients [35].

We start with the SM. At zero γ^5 insertions, the Fano coefficients are:

$$\begin{cases} A^{[0]} &= F^{[0]}(\beta_\tau^2 z^2 - \beta_\tau^2 + 2) \\ \tilde{B}_r^{[0]} &= F_B^{[0]} \sqrt{1-z^2} \sqrt{1-\beta_\tau^2} \\ \tilde{B}_n^{[0]} &= 0 \\ \tilde{B}_k^{[0]} &= -F_B^{[0]} z \\ \tilde{C}_{rr}^{[0]} &= -F^{[0]}(\beta_\tau^2 - 2)(1-z^2) \\ \tilde{C}_{nn}^{[0]} &= -F^{[0]} \beta_\tau^2 (1-z^2) \\ \tilde{C}_{kk}^{[0]} &= F^{[0]}(\beta_\tau^2 - (\beta_\tau^2 - 2)z^2) \\ \tilde{C}_{kr}^{[0]} &= 2F^{[0]} \sqrt{1-\beta_\tau^2} z \sqrt{1-z^2} \end{cases}, \quad (4.9)$$

where the common factors are

$$F^{[0]} = 4Ne^4 \left(Q_\tau^2 Q_f^2 + 8\Re \left(\frac{Q_\tau Q_f Q_{V\tau} Q_{Vf} m_\tau^2}{D_Z} \right) + \frac{16Q_{V\tau}^2 (Q_{Vf}^2 + Q_{Af}^2) m_\tau^4}{|D_Z|^2} \right), \quad (4.10)$$

$$F_B^{[0]} = 64Ne^4 \left(\Re \left(\frac{Q_{Af} Q_{V\tau} Q_f Q_\tau m_\tau^2}{D_Z} \right) + 4 \frac{Q_{Af} Q_{Vf} Q_{V\tau}^2 m_\tau^4}{|D_Z|^2} \right), \quad (4.11)$$

with N the normalisation factor in eq. (3.2), and $D_Z = c_W s_W (4m_\tau^2 - (1 - \beta_\tau^2)(m_Z^2 - im_Z \Gamma_Z))$ the boosted propagator of the Z boson, together with the electroweak mixing angles coming from the coupling to fermions. These results agree with Ref. [18].

At one insertion of γ^5 , we see the first absorptive contributions, noted by the Γ subscript. They do not share the same common factor with the rest of the coefficients, and disappear as $\Gamma \rightarrow 0$:

$$\begin{cases} A^{[1]} &= 2F^{[1]} z \\ \tilde{B}_n^{[1]} &= F_{\Gamma,B}^{[1]} \sqrt{1-\beta_\tau^2} \sqrt{1-z^2} \\ \tilde{B}_r^{[1]} &= F_B^{[1]} \sqrt{1-\beta_\tau^2} z \sqrt{1+z^2} \\ \tilde{B}_k^{[1]} &= F_B^{[1]} (1+z^2) \\ \tilde{C}_{kk}^{[1]} &= 2F^{[1]} z \\ \tilde{C}_{nr}^{[1]} &= F_\Gamma^{[1]} (1-z^2) \\ \tilde{C}_{nk}^{[1]} &= -F_\Gamma^{[1]} \sqrt{1-\beta_\tau^2} z \sqrt{1-z^2} \\ \tilde{C}_{rk}^{[1]} &= F^{[1]} \sqrt{1-\beta_\tau^2} \sqrt{1-z^2} \end{cases}, \quad (4.12)$$

$$F^{[1]} = 16N Q_{A\tau} Q_{Af} Q_{A\tau} \beta_\tau e^4 \left(2\Re \left(\frac{Q_\tau Q_f m_\tau^2}{D_Z} + \frac{16Q_{V\tau}^2 Q_{Vf} m_\tau^4}{|D_Z|^2} \right) \right), \quad (4.13)$$

$$F_B^{[1]} = 32Ne^4 \beta_\tau Q_{A\tau} \left(\Re \left(\frac{Q_{Vf} Q_f Q_\tau m_\tau^2}{D_Z} \right) + 4 \frac{Q_{V\tau} (Q_{Vf}^2 + Q_{Af}^2) m_\tau^4}{|D_Z|^2} \right),$$

$$F_\Gamma^{[1]} = 32Ne^4 \beta_\tau \Im \left(\frac{Q_{A\tau} Q_{V\tau} Q_f Q_\tau c_W^2 s_W^2 m_\tau^2}{D_Z} \right),$$

$$F_{\Gamma,B}^{[1]} = F_\Gamma^{[1]} \text{ with } (Q_{Vf} \rightarrow Q_{Af}). \quad (4.14)$$

The contributions from double γ^5 insertions are, in agreement with Ref. [18]:

$$\begin{cases} A^{[2]} &= F^{[2]}(1 + z^2) \\ B_k^{[2]} &= F_B^{[2]}z \\ C_{nn}^{[2]} &= F^{[2]}(1 - z^2) \\ C_{rr}^{[2]} &= -F^{[2]}(1 - z^2) \\ C_{kk}^{[2]} &= F^{[2]}(1 + z^2) \end{cases}, \quad (4.15)$$

$$F^{[2]} = 64Ne^4 Q_{A\tau}^2 \beta_\tau^2 \frac{(Q_{Vf}^2 + Q_{Af}^2)m_\tau^4}{|D_Z|^2}, \quad (4.16)$$

$$F_B^{[2]} = -256Ne^4 \Re \left(\frac{Q_{Af} Q_{Vf} Q_{A\tau}^2 m_\tau^4}{|D_Z|^2} \right). \quad (4.17)$$

We now pass to the dipole contribution. They were first derived in [77], and similarly to the SM, we find additional absorptive contributions that are linear in Γ_Z ; moreover we consider complex couplings, unlike [77] which focused on real couplings only.

At one dipole insertion (*i.e.* one insertion of $\sigma^{\mu\nu}$), only zero or one γ^5 insertions are possible. At zero insertions we get

$$\begin{cases} A^{[6,0]} &= F^{[6,0]} \\ \tilde{B}_r^{[6,0]} &= F_B^{[6,0]} \frac{\beta_\tau^2 - 2}{\sqrt{1 - \beta_\tau^2}} \sqrt{1 - z^2} - F_{\Gamma,B}^{[6,0]} \frac{z\sqrt{1 - z^2}}{\sqrt{1 - \beta_\tau^2}} \\ \tilde{B}_n^{[6,0]} &= F_B^{[6,0]} \frac{\beta_\tau}{\sqrt{1 - \beta_\tau^2}} \sqrt{1 - z^2} - F_{\Gamma,B}^{[6,0]} \frac{z\sqrt{1 - z^2}\beta_\tau}{\sqrt{1 - \beta_\tau^2}} \text{ with } (\Re(c_{\gamma/Z}) \leftrightarrow \Im(c_{\gamma/Z})) \\ \tilde{B}_k^{[6,0]} &= 2F_B^{[6,0]}z - F_{\Gamma,B}^{[6,0]}(1 - z^2) \\ \tilde{C}_{rr}^{[6,0]} &= F^{[6,0]}(1 - z^2) \\ \tilde{C}_{kk}^{[6,0]} &= F^{[6,0]}z^2 \\ \tilde{C}_{rn}^{[6,0]} &= F^{[6,0]} \frac{\beta_\tau}{2}(1 - z^2) \text{ with } (\Re(c_{\gamma/Z}) \rightarrow \Im(c_{\gamma/Z})) \\ \tilde{C}_{rk}^{[6,0]} &= F^{[6,0]} \frac{2 - \beta_\tau^2}{2\sqrt{1 - \beta_\tau^2}} z\sqrt{1 - z^2} - F_\Gamma^{[6,0]} \frac{\sqrt{1 - z^2}}{\sqrt{1 - \beta_\tau^2}} \\ \tilde{C}_{nk}^{[6,0]} &= F^{[6,0]} \frac{\beta_\tau^2 \sqrt{1 - z^2}}{\sqrt{1 - \beta_\tau^2}} + F_\Gamma^{[6,0]} \frac{\beta_\tau z\sqrt{1 - z^2}}{2\sqrt{1 - \beta_\tau^2}} \text{ with } (\Re(c_{\gamma/Z}) \leftrightarrow \Im(c_{\gamma/Z})) \end{cases}, \quad (4.18)$$

$$F_{\Gamma}^{[6,0]} = 16\sqrt{2}Ne^3 \frac{m_\tau v}{\Lambda^2} \left(\Re(c_\gamma) Q_f^2 Q_\tau - \Re(c_Z) \frac{16c_W s_W Q_{V\tau} (Q_{Af}^2 + Q_{Vf}^2) m_\tau^4}{|D_Z|^2} \right. \quad (4.19)$$

$$\left. + (\Re(c_\gamma) Q_{V\tau} - \Re(c_Z) Q_\tau c_W s_W) \Re \left(\frac{4Q_{Vf} Q_f m_\tau^2}{D_Z} \right) \right),$$

$$F_{\Gamma}^{[6,0]} = 8\sqrt{2}Ne^3 \beta_\tau \frac{m_\tau v}{\Lambda^2} \Im (c_\gamma Q_{V\tau} + c_Z Q_\tau c_W s_W) \Im \left(\frac{Q_{Af} Q_f m_\tau^2}{D_Z} \right), \quad (4.20)$$

$$F_B^{[6,0]} = 8\sqrt{2}Ne^3 \beta_\tau \frac{m_\tau v}{\Lambda^2} \left(Q_{Af} Q_f (\Re(c_\gamma) Q_{V\tau} + \Re(c_Z) Q_\tau c_W s_W) \Re \left(\frac{m_\tau^2}{D_Z} \right) \right. \quad (4.21)$$

$$\left. + 8Q_{Af} Q_{Vf} Q_{V\tau} \Re(c_Z) \frac{m_\tau^4}{|D_Z|^2} \right),$$

$$F_{\Gamma,B}^{[6,0]} = F_{\Gamma}^{[6,0]} \text{ with } (Q_{Af} \rightarrow Q_{Vf}). \quad (4.22)$$

At one insertion of both γ^5 and $\sigma^{\mu\nu}$, we obtain⁶

$$\left\{ \begin{array}{ll} A^{[6,1]} &= F^{[6,1]} z \\ \tilde{B}_r^{[6,1]} &= F_B^{[6,1]} \frac{z\sqrt{1-z^2}}{\sqrt{1-\beta_\tau^2}} + F_{\Gamma,B}^{[6,1]} \frac{\beta_\tau}{\sqrt{1-\beta_\tau^2}} \sqrt{1-z^2} \\ \tilde{B}_r^{[6,1]} &= F_B^{[6,1]} \frac{z\sqrt{1-z^2}}{\sqrt{1-\beta_\tau^2}} + F_{\Gamma,B}^{[6,1]} \frac{1}{\sqrt{1-\beta_\tau^2}} \sqrt{1-z^2} \text{ with } (\Re(c_\gamma) \leftrightarrow \Im(c_\gamma)) \\ \tilde{B}_k^{[6,1]} &= F_B^{[6,1]} (1+z^2) \\ \tilde{C}_{kk}^{[6,1]} &= F^{[6,1]} z \\ \tilde{C}_{nr}^{[6,1]} &= F_{\Gamma}^{[6,1]} (1-z^2) \\ \tilde{C}_{rk}^{[6,1]} &= F^{[6,1]} \frac{\sqrt{1-z^2}}{2\sqrt{1-\beta_\tau^2}} + F_{\Gamma}^{[6,1]} \frac{1}{\sqrt{1-\beta_\tau^2}} z\sqrt{1-z^2} \\ \tilde{C}_{nk}^{[6,1]} &= F^{[6,1]} \frac{\beta_\tau \sqrt{1-z^2}}{2\sqrt{1-\beta_\tau^2}} - F_{\Gamma}^{[6,1]} \frac{\beta_\tau}{\sqrt{1-\beta_\tau^2}} z\sqrt{1-z^2} \text{ with } (\Re(c_{\gamma/Z}) \rightarrow \Im(c_{\gamma/Z})) \end{array} \right. , \quad (4.23)$$

$$F^{[6,1]} = 64\sqrt{2}Ne^3 \left(\frac{m_\tau v}{\Lambda^2} \right) Q_{A\tau} Q_{Af} \beta_\tau m_\tau^2 \left(\Re(c_\gamma) \Re \left(\frac{Q_f m_\tau^2}{D_Z} \right) - \Re(c_Z) \frac{8c_W s_W Q_{V\tau} m_\tau^4}{|D_Z|^2} \right. \quad (4.24)$$

$$\left. + (\Re(c_\gamma) Q_{V\tau} - \Re(c_Z) Q_\tau c_W s_W) \Re \left(\frac{4Q_{Vf} Q_f m_\tau^2}{D_Z} \right) \right),$$

$$F_{\Gamma}^{[6,1]} = 32\sqrt{2}Ne^3 \left(\frac{m_\tau v}{\Lambda^2} \right) Q_{Vf} Q_{A\tau} Q_f \beta_\tau \Re(c_\gamma c_W^2 s_W^2) \Re \left(\frac{m_\tau^2}{D_Z} \right), \quad (4.25)$$

$$F_B^{[6,1]} = 32\sqrt{2}Ne^3 Q_{A\tau} \left(\frac{m_\tau v}{\Lambda^2} \right) \beta_\tau \left(\Re(c_\gamma Q_f Q_{Vf}) \Re \left(\frac{m_\tau^2}{D_Z} \right) + \Re(c_Z) \frac{4c_W s_W (Q_{Vf}^2 + Q_{Af}^2) m_\tau^4}{|D_Z|^2} \right), \quad (4.26)$$

$$F_{\Gamma,B}^{[6,1]} = F_{\Gamma}^{[6,1]} \text{ with } (Q_{Af} \rightarrow Q_{Vf}, \Re(c_\gamma) \rightarrow \Im(c_\gamma)). \quad (4.27)$$

⁶Equation (4.24) corrects a typo in eq. A.9 of Ref.[77], which features the wrong power of m_τ in the numerator of the last term.

For the double insertion of the dipole operators, we find it useful to split contributions by counting the numbers of factors of $\Im(c_{\gamma/Z})$, keeping the same notation above. Indeed, insertion of the imaginary part of the Wilson coefficient are essentially a γ^5 insertion. At zero insertions we recover the results of Ref. [77]:

$$\begin{cases} A^{[8,0]} &= F^{[8,0]}(-\beta_\tau^2 z^2 - \beta_\tau^2 + 2) \\ \tilde{B}_r^{[8,0]} &= F_B^{[8,0]} \frac{\sqrt{1-z^2}}{\sqrt{1-\beta_\tau^2}} \\ \tilde{B}_k^{[8,0]} &= F_B^{[8,0]} z \\ \tilde{C}_{rr}^{[8,0]} &= F^{[8,0]}(2 - \beta_\tau^2)(1 - z^2) \\ \tilde{C}_{nn}^{[8,0]} &= F^{[8,0]} \beta_\tau^2(1 - z^2) \\ \tilde{C}_{kk}^{[8,0]} &= F^{[8,0]}((2 - \beta_\tau^2)z^2 - \beta_\tau^2) \\ \tilde{C}_{rk}^{[8,0]} &= F^{[8,0]} 2\sqrt{1-\beta_\tau^2} z \sqrt{1-z^2} \end{cases}, \quad (4.28)$$

$$\begin{aligned} F^{[8,0]} &= 32N e^2 \left(\frac{m_\tau v}{\Lambda}\right)^2 \frac{1}{1-\beta_\tau^2} \left(Q_f^2 \Re(c_\gamma)^2 - 8\Re(c_\gamma)\Re(c_Z)\Re\left(\frac{Q_f Q_{Vf} m_\tau^2}{D_Z}\right) \right. \\ &\quad \left. + 16\Re(c_\gamma^2) \frac{m_\tau^4 c_W^2 s_W^2 (Q_{Af}^2 + Q_{Vf}^2)}{|D_Z|^2} \right), \\ F_B^{[8,0]} &= 64N e^2 \left(\frac{m_\tau v}{\Lambda}\right)^2 \left(\Re(c_\gamma)\Re(c_Z)\Re\left(\frac{Q_f Q_{Af} m_\tau^2}{D_Z}\right) + 4\Re(c_Z)^2 \frac{m_\tau^4 c_W^2 s_W^2 Q_{Af} Q_{Vf}}{|D_Z|^2} \right) \end{aligned} \quad (4.29)$$

$$(4.30)$$

The imaginary squared contribution is particularly simple; indeed it produces a singlet state $C^{[8,2]} = -A^{[8,2]}\mathbb{1}_3$, with the overall normalisation being

$$A^{[8,2]} = F^{[8,2]} = F^{[8,0]} \beta_\tau^2 (1 - z^2) \text{ with } (\Re(c_{\gamma/Z}) \rightarrow \Im(c_{\gamma/Z})) \quad (4.31)$$

The pure real and pure imaginary contributions produce then two orthogonal spin configuration, which cannot interfere in the cross section:

$$A^{[8,1]} = 0. \quad (4.32)$$

Nonetheless, spin correlations resurrect the interference, and we obtain

$$\begin{cases} \tilde{B}_r^{[8,1]} &= F_{\Gamma,B}^{[8,1]} \frac{z\sqrt{1-z^2}}{\sqrt{1-\beta_\tau^2}} \\ \tilde{B}_n^{[8,1]} &= F^{[8,1]} \frac{\sqrt{1-z^2}}{\sqrt{1-\beta_\tau^2}} \\ \tilde{B}_k^{[8,1]} &= F_{\Gamma,B}^{[8,1]} 1 - z^2 \\ \tilde{C}_{rn}^{[8,1]} &= F^{[8,1]} \frac{1-z^2}{1-\beta_\tau^2} \\ \tilde{C}_{rk}^{[8,1]} &= F_{\Gamma}^{[8,1]} \frac{\sqrt{1-z^2}}{\sqrt{1-\beta_\tau^2}} \\ \tilde{C}_{nk}^{[8,1]} &= F^{[8,1]} \sqrt{1-\beta_\tau^2} z \sqrt{1-z^2} \end{cases}, \quad (4.33)$$

$$F^{[8,1]} = 64Ne^2 \left(\frac{m_\tau v}{\Lambda} \right)^2 \frac{\beta_\tau}{1 - \beta_\tau^2} \left(Q_f^2 \Re(c_\gamma) \Im(c_\gamma) \right. \\ \left. + 4Q_f Q_{Vf} \left(\Re(c_\gamma) \Im(c_Z) + \Re(c_Z) \Im(c_\gamma) \Re\left(\frac{c_W s_W m_\tau^2}{D_Z}\right) \right) + 16 \frac{c_W^4 s_W^4 (Q_{Vf}^2 + Q_{Af}^2) \Re(c_Z) \Im(c_Z) m_\tau^4}{|D_Z|^2} \right), \quad (4.34)$$

$$F_\Gamma^{[8,1]} = 128Ne^2 \left(\frac{m_\tau v}{\Lambda} \right)^2 \beta_\tau \left(Q_f Q_{Af} \Re(c_\gamma) \Im(c_Z) - \Re(c_Z) \Im(c_\gamma) \Im\left(\frac{c_W^3 s_W^3 m_\tau^2}{D_Z}\right) \right) \quad (4.35)$$

$$F_B^{[8,1]} = 256Ne^2 \left(\frac{m_\tau v}{\Lambda} \right)^2 \beta_\tau \left(Q_f Q_{Af} (\Re(c_Z) \Im(c_\gamma) - \Re(c_\gamma) \Im(c_Z)) \Re\left(\frac{c_W s_W m_\tau^2}{D_Z}\right) \right. \\ \left. + 4 \frac{\Re(c_Z) \Im(c_W^4 s_W^4 c_Z) Q_{Af} Q_{Vf} m_\tau^4}{|D_Z|^2} \right), \quad (4.36)$$

$$F_{\Gamma,B}^{[8,1]} = F_\Gamma^{[8,1]} \text{ with } (Q_{Af} \rightarrow Q_{Vf}). \quad (4.37)$$

4.2 Quantum Observable and Spin Correlation

4.2.1 Lepton Colliders

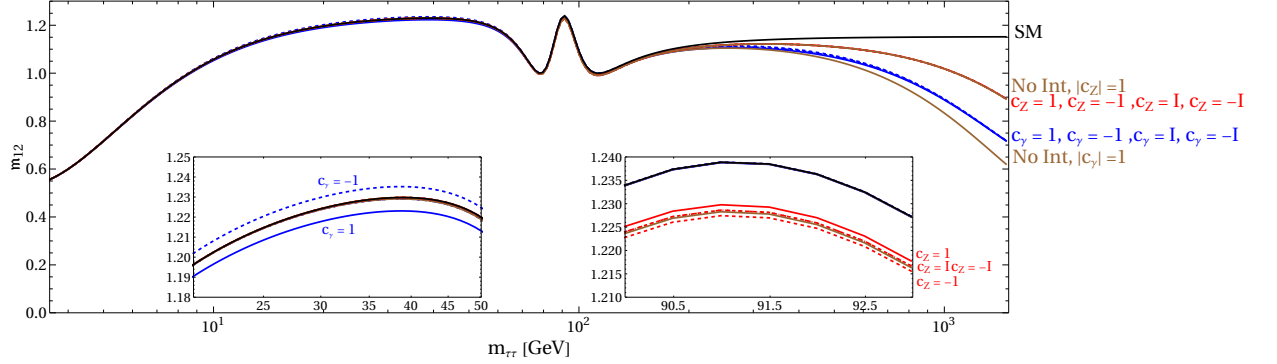


Figure 1. The m_{12} Bell inequality marker for $ee \rightarrow \tau\tau$, $C_{\gamma/Z} = 1/1.5 \text{ TeV}^{-2}$. The insets show the local maxima of entanglement to appreciate the deviations due to the photon dipole operator (around $m_{\tau\tau} = 40 \text{ GeV}$) and Z dipole operator (around $m_{\tau\tau} = m_Z$). For $m_{\ell\ell} \gg m_Z$, the SM approaches a constant value, while the SMEFT operators bring down the entanglement of the tau pair state. Resurrection of interference of the photon dipole can be observed, but the interference and SMEFT squared contributions partially cancel each other. Moreover, while at the local maxima the $c = 1$ and $c = -1$ contributions can be distinguished, this is not true for $m_{\ell\ell} \gg m_Z$; imaginary Wilson coefficients, on the other hand, contribute negligibly at low energies and cannot be distinguished from real coefficients at large energies.

In figs. 1 to 4 we show the spin correlation observables for $ee \rightarrow \tau\tau$, at energies relevant for both past (LEP), current (Belle II), and proposed lepton colliders (FCC-ee, CLIC and ILC). Of course, while we refer to a ee collider, the results for a $\mu\mu$ collider would be exactly the same at the energies we consider here, because in both cases the mass of the initial leptons can be neglected.

In the SM, the maximum amount of entanglement can be observed at energies close to 30-50 GeV, where the photon exchange dominates and the external fermions can be

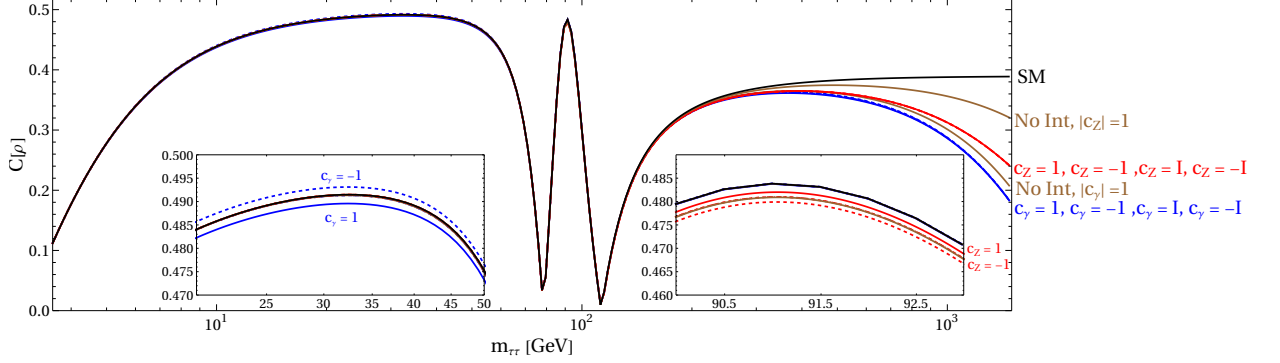


Figure 2. Same as fig. 1, but here the Concurrence $C[\rho]$, which quantifies entanglement directly, is plotted. In this case, resurrection of interference can be observed for both the photon and Z dipole operators, and the interference and SMEFT squared contributions both decrease entanglement. However, at large energies the sign and phase of the Wilson coefficient cannot be determined, and at low energies there is limited sensitivity to the imaginary part of the Wilson coefficients.

considered as massless, and around the Z pole, where the Z -exchange dominates. As a result, around these energies one can observe the largest deviation in the spin correlation observables: adding the γ dipole operator changes the correlation pattern around the first maximum, while it has negligible effect at the Z pole, and vice-versa adding the Z dipole has a clearly observable effect at the Z pole, being a resonant contribution there.

Observing fig. 1, one can notice how resurrection is successful in the Bell inequality marker \mathbf{m}_{12} , in the sense that the interference has a non-negligible effect at large energies, but unfortunately the effect is to reduce the difference with the SM, making the observable less sensitive compared to if resurrection did not occur. Moreover, at large energies the phase of the Wilson coefficient does not make any significant difference in the Bell inequality violation. Around the first maximum, however, the phase does play a role, with the pure imaginary coupling (hence CP -violating) benchmark increasing the amount of Bell inequality violation, and the opposite happening for pure real couplings (CP -conserving).

We show the concurrence in fig. 2. We have a similar situation regarding the phase of the Wilson coefficient, but unlike the case of \mathbf{m}_{12} , here the interference contribution are actually of the same sign as the SMEFT squared, allowing for increased sensitivity thanks to resurrection.

Since the concurrence is a finer discriminant of quantum correlation than Bell inequality violation, one might imagine that the quantum discord, being an even finer discriminant, might fare even better as a NP probe. This is not the case, as can be seen in fig. 3: just like the case of \mathbf{m}_{12} , the interference contributions for the LQU have opposite sign as the SMEFT squared contributions. It is interesting to note how the LQU features a maximum at small energies that is absent from the entanglement markers, as well as the fact that there is an increase in LQU when the SMEFT operators are added, while entanglement and Bell inequality violation fall off.

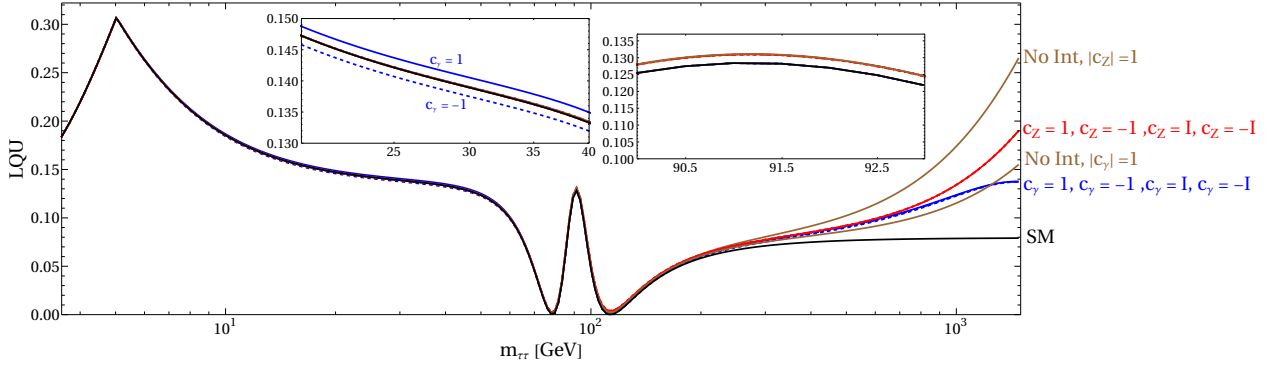


Figure 3. Same as fig. 1, but for the LQU, which quantifies quantum discord. The conclusions are mostly similar as in fig. 1, but resurrection of interference can be observed for the Z dipole, as well.

Finally, we consider the elements of the C matrix. In fig. 4, we plot the (nk) element of the C matrix. In the SM, this entry receives only a contribution proportional to the imaginary part of the Z propagator, which is small with respect to A anywhere but around the Z resonance. Moreover, no contribution from SMEFT squared is present, except in the interference between CP conserving and CP violating dipole moments, and thus C_{nk} is a perfect candidate to measure the sign and phase of the Wilson coefficients. Only the real part of the Wilson coefficients contributes in the high-energy limit and indeed the lines for pure imaginary coupling deviate negligibly from the SM except around the Z pole. It should be noted that, at high energy, information about the sign of the Wilson coefficient is lost, partially explaining the similar phenomenon in the quantum information observables. However, unlike the quantum observables, sizable deviations from the SM can be observed at lower energies, as well as separation between the lines belonging to different sign. It should be noted that, if we considered the (r, k) element instead, the roles of the imaginary and real part of the Wilson coefficient would be switched. This makes it straightforward to experimentally disentangle the phase of the Wilson coefficient, as real and imaginary part contribute to different entries of the spin correlation matrix. On the other hand, the quantum observables, being a combination of all the spin observables, lose differentiating power between the different scenarios for the phase.

4.2.2 SMEFT Sensitivity

To compare the different observables as a NP probe, we show in fig. 5 their sensitivity at three benchmark energies, namely $m_{\ell\ell} = 10.56$ GeV, m_Z , 500 GeV. The first energy is the $\Upsilon(4S)$ resonance at which Belle II operates, while the other two are relevant for a TeraZ machine and one of the proposed working energies for future lepton colliders. For Belle II, we use the uncertainties derived from MC simulations in Ref. [43], which considered 200 million events. For the TeraZ machine, we rescale the uncertainties estimated in [78] by a factor $10\sqrt{50}$ to reach the expected 100 million events. Finally, for the lepton collider at 500 GeV we rescale the TeraZ uncertainty by the square root of cross section, as suggested

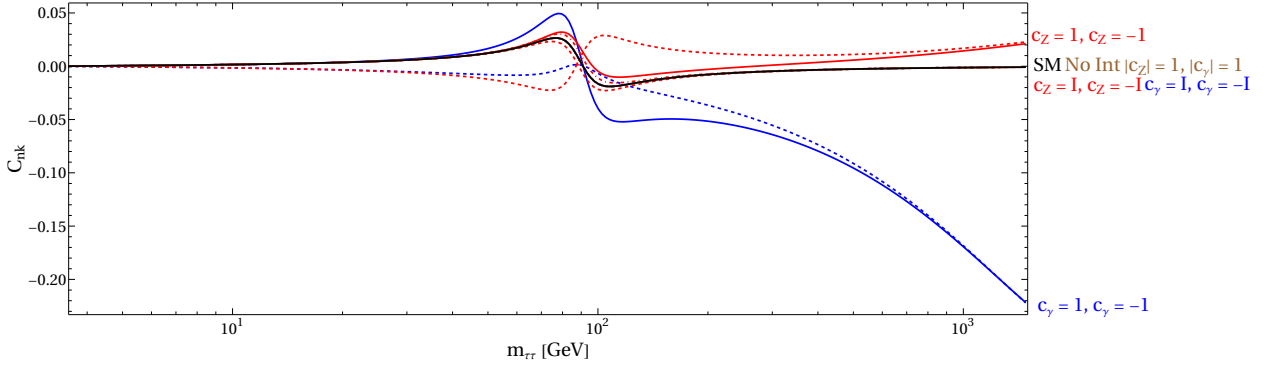


Figure 4. Same as fig. 1, but for the (nk) element of the spin correlation matrix. Unlike the quantum information observables, here the SMEFT squared contribution is negligible, and the interference gives the leading deviation from the SM. Moreover, the sign of the real part of the Wilson coefficient changes dramatically the shape of the curve, everywhere but near the NP scale Λ . Note that the imaginary part of the Wilson coefficient contributes modestly to negligibly, but the roles of imaginary and real parts are exchanged in the (nr) element, such that the phase of the Wilson coefficient can be obtained by examining all the elements of the C matrix.

in [77]. For the spin correlation matrix, we consider at each benchmark point only the element that provides the greatest deviation from the SM. At all benchmark energies, we also show the reach of the total cross section σ , taking into consideration only statistical uncertainty.

It is clear from fig. 5 that, at energies high enough to be sensitive to the CP violation in the EW theory, the quantum information observables diminish the sensitivity with no advantage. At Belle II energies, the concurrence has a slightly better sensitivity for real couplings compared to the spin correlations, but at the price of significantly worse sensitivity for imaginary couplings. Moreover, the bounds are derived from one single element of the C matrix; the sensitivity can be enhanced by considering more than one entry, as well as the polarisation vectors B . Thus, we argue that the quantum observables perform worse in resurrections scenarios, and the strongest bounds are instead provided by the spin correlation matrix directly.

Quantum information observables do not display increased sensitivity to the phase of the Wilson coefficient, and are unable to distinguish CP conserving and violating scenarios. Due to their definition, which involves taking the eigenvalues of a 3×3 matrix, understanding analytically the reason behind these facts is challenging. The C matrix coefficients, instead, can be easily calculated and interpreted. Experimentally, measuring the C matrix is needed to reconstruct the density matrix, so there seems to be no advantage in using quantum information observables in this scenario.

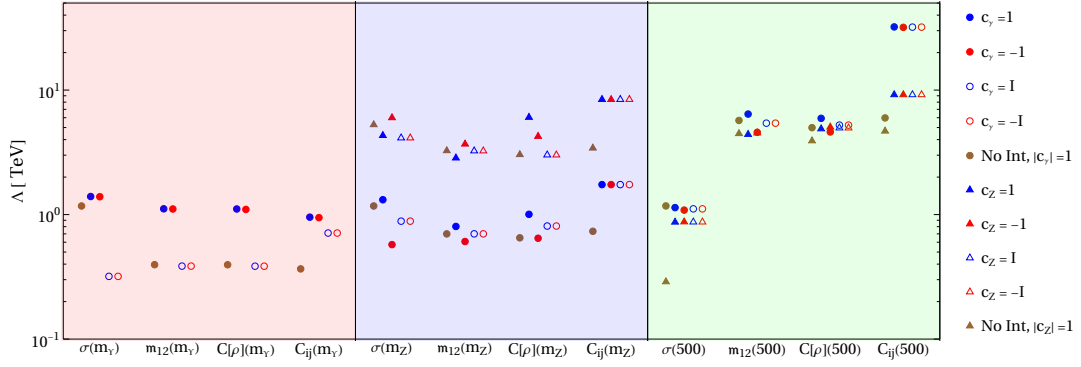


Figure 5. 95% CL sensitivity on the new physics scale Λ for the $\mathcal{O}_{\tau V}$ operators, derived from measurements of the total cross section, as well as different spin correlation observables at three benchmark energies. Quantum information observables perform similarly or better than the single coefficient of the C matrix at Belle-II energies, where the photon dominates and there is no CP violation, but become progressively less effective at higher energies, performing poorly compared to the spin correlation coefficient. NP scales lower than the EW scale are not plotted.

4.2.3 Hadron Colliders

At hadron colliders, the LO prediction at partonic level has to be weighted by the PDF of the partons, as explained in section 3. Figures 6 to 9 are the analogue of figs. 1 to 4, and the same patterns can be seen regarding resurrection of interference. Namely, the net effect of the resurrection phenomenon in the Bell inequality marker m_{12} and the local quantum uncertainty LQU is to decrease the sensitivity to the NP scale Λ . For the concurrence $C[\rho]$ the resurrection phenomenon improves the sensitivity, but only for real Wilson coefficients. In the spin correlation matrix elements, instead resurrection improves the sensitivity, both for real and imaginary Wilson coefficients.

As mentioned in section 3.2, the measurement of spin correlations at hadron colliders is much more involved than at lepton colliders. Indeed, while at lepton colliders the ambiguity due to the non-measurement of neutrinos can be resolved using impact parameters [45], the same task is made more difficult at hadron colliders by the lack of knowledge of the c.o.m. frame. Measurements at resonances, such as $m_{\ell\ell} = m_Z(m_H)$ can partially circumvent this difficulty by assuming the process predominantly occurs via on-shell $Z(H)$ decay [79]. Indeed, a measurement of the τ polarisation has recently been performed at the CMS experiment, using a sample with an integrated luminosity of 36.3 fb^{-1} [80]. Different strategies have been devised to boost the reconstruction efficiency for the τ momentum, including matrix element [81] and machine learning [82–84] techniques, and a dedicated algorithm to calculate the spin correlation coefficients at hadron collider exists [85].

Given the difficulties posed by a measurement of polarisations at collider, we do not try here to estimate the experimental uncertainty on the spin correlation coefficients. Instead, we report the uncertainty that a Z-pole measurement should have to reach the benchmark bound $C_\gamma \lesssim 1/1.5 \text{ TeV}^2$, obtained from high-energy measurement of the cross section. That is, to be competitive with the limit reported in Ref. [47] at 95%CL, the uncertainty

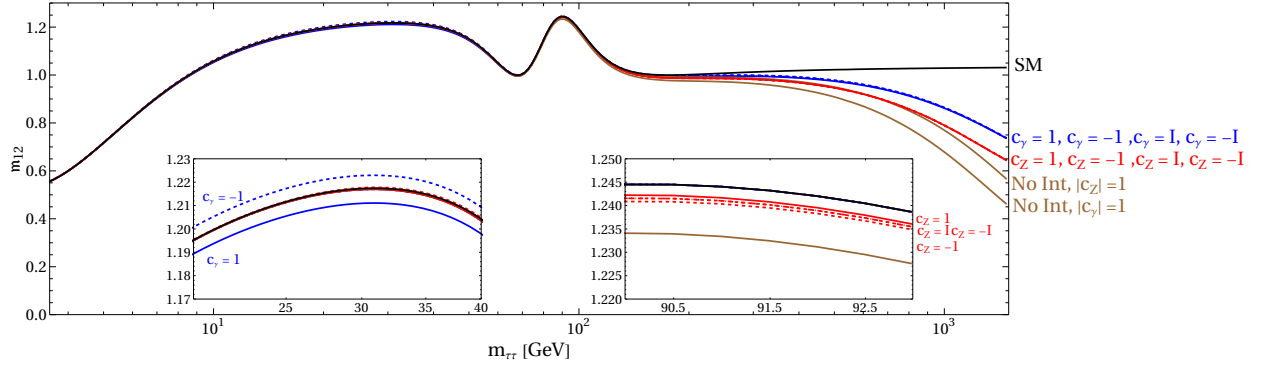


Figure 6. Same as fig. 1, but for pp initial state.

$\delta C(\delta B)$ on the entries of $C(B)$ need to satisfy

$$\begin{aligned} \delta B &< 0.0005 \\ \delta C &< 0.008, \end{aligned} \tag{4.38}$$

to be contrasted with the current uncertainty of $\delta B_{\text{CMS}} = 0.015$ [80]. Similarly to the ee case, the phase of the Wilson coefficient can be determined by measuring all the entries of B and C . For the weak dipole, an exclusion of $C_Z \lesssim 1/1.5 \text{ TeV}^{-2}$ is expected if the following experimental uncertainties can be reached

$$\begin{aligned} \delta B &< 0.003 \\ \delta C &< 0.03. \end{aligned} \tag{4.39}$$

5 Conclusions and Outlook

In this paper we explored interference resurrection in 4-fermion scattering by measuring the final-state angular correlations, and the resulting improvement in sensitivity to SMEFT operators. We find that, at moderate and large energies compared to the EW scale, spin observables greatly outperform the cross section in sensitivity. We also consider quantum information observables, which have obtained considerable attention lately in the top sector, and have been shown to outperform other angular observables as a probe of SMEFT operators [18]. We compare the sensitivity on the new physics scale Λ for γ or Z dipole operators, in fig. 5, and find that there is no advantage in employing quantum observables like the concurrence $C[\rho]$, the Bell inequality violation marker m_{12} or the local quantum uncertainty LQU. Indeed, classical spin correlations significantly improve the sensitivity in comparison to both cross-section measurement and quantum information observables. As we show in figs. 1 to 4 for the ee case and figs. 6 to 9 for the pp case, the resurrection is only partially successful in the quantum information observables, because phase information

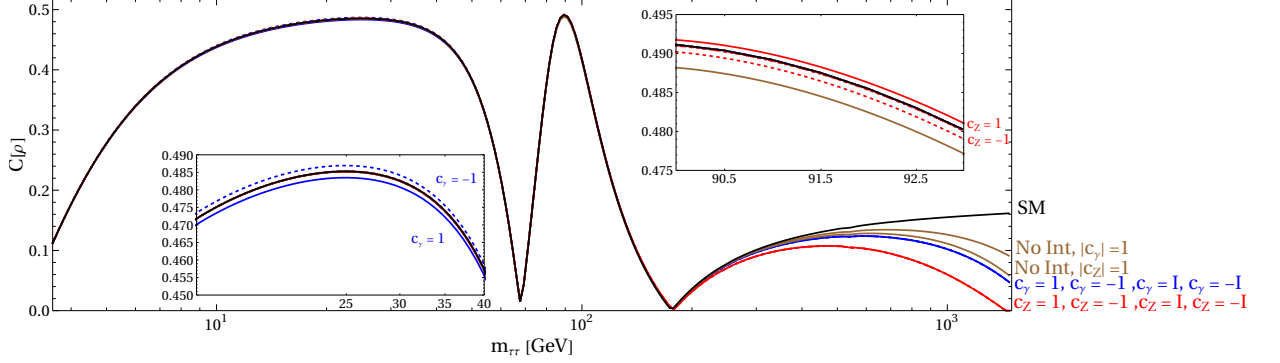


Figure 7. Same as fig. 2, but for pp initial state.

is lost, and in some cases the interference partially cancels against the SMEFT squared contribution.

We believe that these results in the $\tau\tau$ case differ from the top pair case because top pair production respects CP , C and P parities to a good approximation [10], which imposes a quite simple spin state. In this case, entanglement can be directly extracted from the diagonal entries of the spin correlation matrix C . However, as we observed in section 2.1, resurrection of interference only involves the off-diagonal entries of the C matrix, so the simplified entanglement markers do not participate in resurrection. Moreover, the violation of P and C symmetries makes the simplified criterion for entanglement used in [18] only a sufficient, but not necessary, condition for entanglement. More appropriate entanglement markers are \mathbf{m}_{12} and $C[\rho]$, that distill the R matrix to a single number, thus losing the ability to differentiate the different off-diagonal components of the C matrix. In addition, the relatively complicated expression of \mathbf{m}_{12} and $C[\rho]$, involving the eigenvalues of a 3×3 matrix, hinder an analytical understanding of how exactly the quantum information observables relate to the underlying spin coefficients. We can nonetheless observe in figs. 1 to 4 and 6 to 9 that CP information is mostly lost in the quantum information observables at high energies, while the spin correlation coefficients retain it. This supports the hypothesis that CP violation is why QCD top pair production is different than EW $\tau\tau$ production. Since the spin correlation coefficients are anyway the building blocks for any quantum information study, they seem like a much more appropriate choice as NP probes.⁷

Looking forward, the identification of optimal observables for the set of operators discussed in this work is an important endeavor. For this goal, a full estimation of the sensitivity of current and proposed colliders to spin correlation is necessary. While studies for lepton collider are abundant, fewer exist for hadron collider, due to the known difficulty of correctly reconstructing the final particles' 4-momentum when invisible particles are present in their decay. Recent efforts [81–85] might change the situation, but the needed

⁷We again stress the difference with top quark pair production, where the Peres-Horodecki criterion allows direct measurement of entanglement, without necessarily measuring the C matrix elements [11].

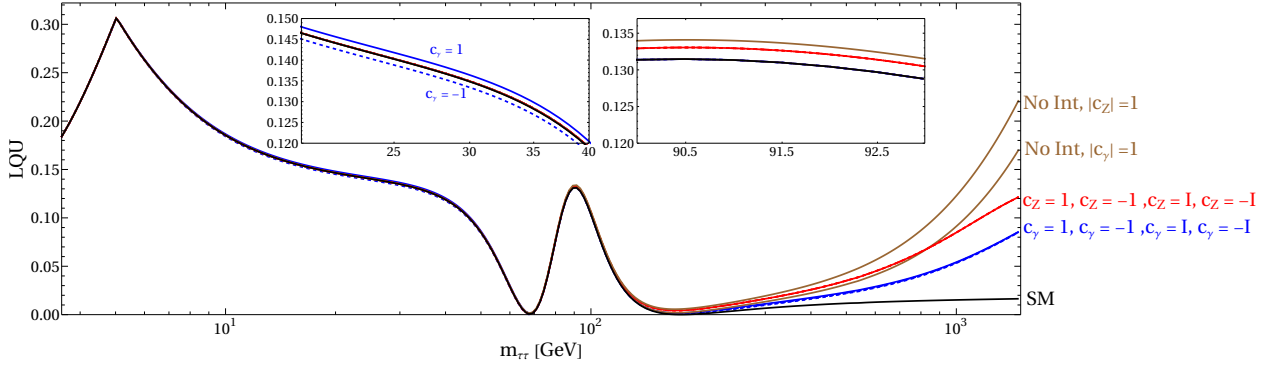


Figure 8. Same as fig. 3, but for pp initial state.

sensitivities to be competitive with cross-section measurements seem at this time far in the future, see eq. (4.38) and the discussion around it.

All the calculations performed in this work are at tree-level, given that the effect of NLO is expected to be small, as spin correlations are ratios of cross sections. Nonetheless, it would be interesting to understand the effect of soft radiation and loop effects. Interestingly, one expects the properly resummed tree-level answer, corresponding a classical field theory, not to exhibit entanglement at all. Thus, if the LO calculation is to be close to the exact one, it seems like quantum correction, on their own, would work to increase entanglement. The interplay of quantum correction and soft radiation merits further discussion.

Entanglement has also been proposed as a guiding principle for parameter selection through the emergence of global symmetries via a sort of stationary principle for entanglement [77, 86–90]. While enticing, most of these proposals either rely on specific angular configurations or additional assumptions, so at the current state it is hard to establish a general principle and more information is needed. In this paper, we add another piece to the puzzle by studying the LQU, a discord-like measure for non-classical correlation [40]. As can be seen in figs. 3 and 8, the LQU has a local maximum that is absent in the entanglement markers, and cannot be easily explained by the presence of a symmetry or resonance. While other measures of quantum discord have already been considered in the literature [39], their simplified definition used so far can only be applied to the simple spin state of the top, and the complete case involves a complicated minimisation procedure. In contrast, the LQU has an explicit formula that is applicable to any bipartite qubit [40], so its use facilitates studies of non-classical correlations beyond entanglement. It will be interesting to study the robustness of the principles proposed in [86–88] on measure of non-classicality that go beyond entanglement using the LQU.

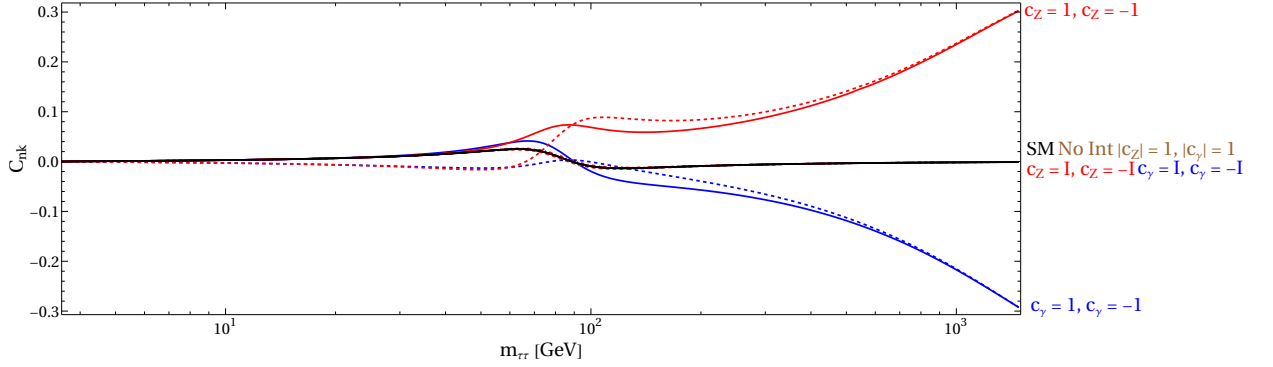


Figure 9. Same as fig. 4, but for pp initial state.

Acknowledgments

The author is very grateful to Felix Yu for many useful discussions. The author acknowledges a conversation with Miki Chala about resurrection. The author would like to thank Felix Yu and Sebastian Schenk for feedback on the manuscript. The author would also like to thank the Fermilab theory group for their kind hospitality while this work was in progress. This work was supported by the Cluster of Excellence *Precision Physics, Fundamental Interactions and Structure of Matter* (PRISMA⁺ – EXC 2118/1) within the German Excellence Strategy (project ID 390831469).

References

- [1] W. Buchmuller and D. Wyler, *Effective Lagrangian Analysis of New Interactions and Flavor Conservation*, *Nucl. Phys. B* **268** (1986) 621–653.
- [2] I. Brivio and M. Trott, *The Standard Model as an Effective Field Theory*, *Phys. Rept.* **793** (2019) 1–98, [[arXiv:1706.08945](#)].
- [3] A. Falkowski, M. Gonzalez-Alonso, A. Greljo, D. Marzocca, and M. Son, *Anomalous Triple Gauge Couplings in the Effective Field Theory Approach at the LHC*, *JHEP* **02** (2017) 115, [[arXiv:1609.06312](#)].
- [4] D. Liu, A. Pomarol, R. Rattazzi, and F. Riva, *Patterns of Strong Coupling for LHC Searches*, *JHEP* **11** (2016) 141, [[arXiv:1603.03064](#)].
- [5] A. Azatov, R. Contino, C. S. Machado, and F. Riva, *Helicity selection rules and noninterference for BSM amplitudes*, *Phys. Rev. D* **95** (2017), no. 6 065014, [[arXiv:1607.05236](#)].
- [6] A. Helset and M. Trott, *On interference and non-interference in the SMEFT*, *JHEP* **04** (2018) 038, [[arXiv:1711.07954](#)].
- [7] A. Azatov, D. Barducci, and E. Venturini, *Precision diboson measurements at hadron colliders*, *JHEP* **04** (2019) 075, [[arXiv:1901.04821](#)].

- [8] H. El Faham, G. Pelliccioli, and E. Vryonidou, *Triple-gauge couplings in LHC diboson production: a SMEFT view from every angle*, [arXiv:2405.19083](#).
- [9] L. J. Dixon and Y. Shadmi, *Testing gluon selfinteractions in three jet events at hadron colliders*, *Nucl. Phys. B* **423** (1994) 3–32, [[hep-ph/9312363](#)]. [Erratum: Nucl.Phys.B 452, 724–724 (1995)].
- [10] Y. Afik and J. R. M. n. de Nova, *Entanglement and quantum tomography with top quarks at the LHC*, *Eur. Phys. J. Plus* **136** (2021), no. 9 907, [[arXiv:2003.02280](#)].
- [11] **ATLAS** Collaboration, G. Aad et al., *Observation of quantum entanglement in top-quark pairs using the ATLAS detector*, [arXiv:2311.07288](#).
- [12] A. J. Barr, M. Fabbrichesi, R. Floreanini, E. Gabrielli, and L. Marzola, *Quantum entanglement and Bell inequality violation at colliders*, [arXiv:2402.07972](#).
- [13] J. S. Bell, *On the Einstein-Podolsky-Rosen paradox*, *Physics Physique Fizika* **1** (1964) 195–200.
- [14] S. J. Freedman and J. F. Clauser, *Experimental test of local hidden-variable theories*, *Phys. Rev. Lett.* **28** (Apr, 1972) 938–941.
- [15] J. F. Clauser, M. A. Horne, A. Shimony, and R. A. Holt, *Proposed experiment to test local hidden-variable theories*, *Phys. Rev. Lett.* **23** (Oct, 1969) 880–884.
- [16] S. A. Abel, M. Dittmar, and H. K. Dreiner, *Testing locality at colliders via Bell’s inequality?*, *Phys. Lett. B* **280** (1992) 304–312.
- [17] S. Li, W. Shen, and J. M. Yang, *Can Bell inequalities be tested via scattering cross-section at colliders ?*, [arXiv:2401.01162](#).
- [18] F. Maltoni, C. Severi, S. Tentori, and E. Vryonidou, *Quantum detection of new physics in top-quark pair production at the LHC*, *JHEP* **03** (2024) 099, [[arXiv:2401.08751](#)].
- [19] B. Grzadkowski, M. Iskrzynski, M. Misiak, and J. Rosiek, *Dimension-Six Terms in the Standard Model Lagrangian*, *JHEP* **10** (2010) 085, [[arXiv:1008.4884](#)].
- [20] E. H. Simmons, *Dimension-six Gluon Operators as Probes of New Physics*, *Phys. Lett. B* **226** (1989) 132–136.
- [21] E. H. Simmons, *Higher dimension gluon operators and hadronic scattering*, *Phys. Lett. B* **246** (1990) 471–476.
- [22] A. Azatov, J. Elias-Miro, Y. Reyimuaji, and E. Venturini, *Novel measurements of anomalous triple gauge couplings for the LHC*, *JHEP* **10** (2017) 027, [[arXiv:1707.08060](#)].
- [23] R. Aoude and W. Shepherd, *Jet Substructure Measurements of Interference in Non-Interfering SMEFT Effects*, *JHEP* **08** (2019) 009, [[arXiv:1902.11262](#)].
- [24] G. Panico, F. Riva, and A. Wulzer, *Diboson interference resurrection*, *Phys. Lett. B* **776** (2018) 473–480, [[arXiv:1708.07823](#)].
- [25] G. M. D’Ariano, M. G. A. Paris, and M. F. Sacchi, *Quantum Tomography*, [quant-ph/0302028](#).
- [26] Y. Afik and J. R. M. n. de Nova, *Quantum information with top quarks in QCD*, *Quantum* **6** (2022) 820, [[arXiv:2203.05582](#)].
- [27] U. Fano, *Pairs of two-level systems*, *Rev. Mod. Phys.* **55** (1983) 855–874.

- [28] **PDF4LHC Working Group** Collaboration, R. D. Ball et al., *The PDF4LHC21 combination of global PDF fits for the LHC Run III*, *J. Phys. G* **49** (2022), no. 8 080501, [[arXiv:2203.05506](#)].
- [29] D. Clark, E. Godat, and F. Olness, *Maneparse: a mathematica reader for parton distribution functions*, *Computer Physics Communications* (2016).
- [30] E. Schrödinger, *Discussion of probability relations between separated systems*, *Mathematical Proceedings of the Cambridge Philosophical Society* **31** (1935), no. 4 555–563.
- [31] R. Horodecki, P. Horodecki, M. Horodecki, and K. Horodecki, *Quantum entanglement*, *Reviews of Modern Physics* **81** (jun, 2009) 865–942.
- [32] W. K. Wootters, *Entanglement of formation of an arbitrary state of two qubits*, *Physical Review Letters* **80** (mar, 1998) 2245–2248.
- [33] R. Horodecki, P. Horodecki, and M. Horodecki, *Violating bell inequality by mixed spin-1/2 states: necessary and sufficient condition*, *Physics Letters A* **200** (1995), no. 5 340–344.
- [34] N. Gisin, *Bell’s inequality holds for all non-product states*, *Physics Letters A* **154** (1991), no. 5 201–202.
- [35] W. Bernreuther, D. Heisler, and Z.-G. Si, *A set of top quark spin correlation and polarization observables for the LHC: Standard Model predictions and new physics contributions*, *JHEP* **12** (2015) 026, [[arXiv:1508.05271](#)].
- [36] A. Peres, *Separability criterion for density matrices*, *Phys. Rev. Lett.* **77** (1996) 1413–1415, [[quant-ph/9604005](#)].
- [37] C. H. Bennett, D. P. DiVincenzo, C. A. Fuchs, T. Mor, E. Rains, P. W. Shor, J. A. Smolin, and W. K. Wootters, *Quantum nonlocality without entanglement*, *Phys. Rev. A* **59** (1999) 1070, [[quant-ph/9804053](#)].
- [38] A. Bera, T. Das, D. Sadhukhan, S. S. Roy, A. S. De, and U. Sen, *Quantum discord and its allies: a review*, *arXiv preprint arXiv: 1703.10542* (2017).
- [39] Y. Afik and J. R. M. n. de Nova, *Quantum Discord and Steering in Top Quarks at the LHC*, *Phys. Rev. Lett.* **130** (2023), no. 22 221801, [[arXiv:2209.03969](#)].
- [40] D. Girolami, T. Tufarelli, and G. Adesso, *Characterizing Nonclassical Correlations via Local Quantum Uncertainty*, *Phys. Rev. Lett.* **110** (2013), no. 24 240402, [[arXiv:1212.2214](#)].
- [41] M. Baumgart and B. Tweedie, *A New Twist on Top Quark Spin Correlations*, *JHEP* **03** (2013) 117, [[arXiv:1212.4888](#)].
- [42] M. M. Altakach, P. Lamba, F. Maltoni, K. Mawatari, and K. Sakurai, *Quantum information and CP measurement in $H \rightarrow \tau^+ \tau^-$ at future lepton colliders*, [[arXiv:2211.10513](#)].
- [43] K. Ehatäht, M. Fabbrichesi, L. Marzola, and C. Veelken, *Probing entanglement and testing Bell inequality violation with $e+e \rightarrow \tau+\tau^-$ at Belle II*, *Phys. Rev. D* **109** (2024), no. 3 032005, [[arXiv:2311.17555](#)].
- [44] K. Cheng, T. Han, and M. Low, *Optimizing fictitious states for Bell inequality violation in bipartite qubit systems with applications to the $t\bar{t}$ system*, *Phys. Rev. D* **109** (2024), no. 11 116005, [[arXiv:2311.09166](#)].
- [45] D. Jeans, *Tau lepton reconstruction at collider experiments using impact parameters*, *Nucl. Instrum. Meth. A* **810** (2016) 51–58, [[arXiv:1507.01700](#)].

- [46] R. Aoude, E. Madge, F. Maltoni, and L. Mantani, *Probing new physics through entanglement in diboson production*, *JHEP* **12** (2023) 017, [[arXiv:2307.09675](#)].
- [47] U. Haisch, L. Schnell, and J. Weiss, *LHC tau-pair production constraints on a_τ and d_τ* , [arXiv:2307.14133](#).
- [48] S. Eidelman and M. Passera, *Theory of the tau lepton anomalous magnetic moment*, [0701260](#).
- [49] F. Feruglio, P. Paradisi, and O. Sumensari, *Implications of scalar and tensor explanations of $R_{D^{(*)}}$* , *JHEP* **11** (2018) 191, [[arXiv:1806.10155](#)].
- [50] I. Doršner, S. Fajfer, A. Greljo, J. F. Kamenik, and N. Košnik, *Physics of leptoquarks in precision experiments and at particle colliders*, *Phys. Rept.* **641** (2016) 1–68, [[arXiv:1603.04993](#)].
- [51] K.-m. Cheung, *Muon anomalous magnetic moment and leptoquark solutions*, *Phys. Rev. D* **64** (2001) 033001, [[hep-ph/0102238](#)].
- [52] I. Doršner, S. Fajfer, and O. Sumensari, *Muon $g - 2$ and scalar leptoquark mixing*, *JHEP* **06** (2020) 089, [[arXiv:1910.03877](#)].
- [53] A. Crivellin and M. Hoferichter, *Consequences of chirally enhanced explanations of $(g - 2)_\mu$ for $h \rightarrow \mu\mu$ and $Z \rightarrow \mu\mu$* , *JHEP* **07** (2021) 135, [[arXiv:2104.03202](#)]. [Erratum: *JHEP* **10**, 030 (2022)].
- [54] T. Aoyama et al., *The anomalous magnetic moment of the muon in the Standard Model*, *Phys. Rept.* **887** (2020) 1–166, [[arXiv:2006.04822](#)].
- [55] **Muon g-2 Collaboration**, B. Abi et al., *Measurement of the Positive Muon Anomalous Magnetic Moment to 0.46 ppm*, *Phys. Rev. Lett.* **126** (2021), no. 14 141801, [[arXiv:2104.03281](#)].
- [56] A. S. Fomin, A. Y. Korchin, A. Stocchi, S. Barsuk, and P. Robbe, *Feasibility of τ -lepton electromagnetic dipole moments measurement using bent crystal at the LHC*, *JHEP* **03** (2019) 156, [[arXiv:1810.06699](#)].
- [57] J. Fu, M. A. Giorgi, L. Henry, D. Marangotto, F. M. Vidal, A. Merli, N. Neri, and J. Ruiz Vidal, *Novel Method for the Direct Measurement of the τ Lepton Dipole Moments*, *Phys. Rev. Lett.* **123** (2019), no. 1 011801, [[arXiv:1901.04003](#)].
- [58] J. Bernabeu, G. A. Gonzalez-Sprinberg, M. Tung, and J. Vidal, *The Tau weak magnetic dipole moment*, *Nucl. Phys. B* **436** (1995) 474–486, [[hep-ph/9411289](#)].
- [59] J. Bernabeu, G. A. Gonzalez-Sprinberg, J. Papavassiliou, and J. Vidal, *Tau anomalous magnetic moment form-factor at super B/ flavor factories*, *Nucl. Phys. B* **790** (2008) 160–174, [[arXiv:0707.2496](#)].
- [60] J. Bernabeu, G. A. Gonzalez-Sprinberg, and J. Vidal, *Tau spin correlations and the anomalous magnetic moment*, *JHEP* **01** (2009) 062, [[arXiv:0807.2366](#)].
- [61] S. Eidelman, D. Epifanov, M. Fael, L. Mercolli, and M. Passera, *τ dipole moments via radiative leptonic τ decays*, *JHEP* **03** (2016) 140, [[arXiv:1601.07987](#)].
- [62] A. Rajaraman, J. N. Howard, R. Riley, and T. M. P. Tait, *The τ Magnetic Dipole Moment at Future Lepton Colliders*, *LHEP* **2** (2019), no. 2 5, [[arXiv:1810.09570](#)].
- [63] **Belle Collaboration**, K. Inami et al., *An improved search for the electric dipole moment of the τ lepton*, *JHEP* **04** (2022) 110, [[arXiv:2108.11543](#)].

- [64] G. A. Gonzalez-Sprinberg, A. Santamaria, and J. Vidal, *Model independent bounds on the tau lepton electromagnetic and weak magnetic moments*, *Nucl. Phys. B* **582** (2000) 3–18, [[hep-ph/0002203](#)].
- [65] **DELPHI** Collaboration, J. Abdallah et al., *Study of tau-pair production in photon-photon collisions at LEP and limits on the anomalous electromagnetic moments of the tau lepton*, *Eur. Phys. J. C* **35** (2004) 159–170, [[hep-ex/0406010](#)].
- [66] I. Galon, A. Rajaraman, and T. M. P. Tait, *$H \rightarrow \tau^+ \tau^- \gamma$ as a probe of the τ magnetic dipole moment*, *JHEP* **12** (2016) 111, [[arXiv:1610.01601](#)].
- [67] **ATLAS** Collaboration, G. Aad et al., *Observation of the $\gamma\gamma \rightarrow \tau\tau$ Process in Pb+Pb Collisions and Constraints on the τ -Lepton Anomalous Magnetic Moment with the ATLAS Detector*, *Phys. Rev. Lett.* **131** (2023), no. 15 151802, [[arXiv:2204.13478](#)].
- [68] **CMS** Collaboration, A. Tumasyan et al., *Observation of τ lepton pair production in ultraperipheral lead-lead collisions at $\sqrt{s_{NN}} = 5.02$ TeV*, *Phys. Rev. Lett.* **131** (2023) 151803, [[arXiv:2206.05192](#)].
- [69] M. Verducci, N. Vignaroli, C. Roda, and V. Cavasinni, *A study of the measurement of the τ lepton anomalous magnetic moment in high energy lead-lead collisions at LHC*, [[arXiv:2307.15160](#)].
- [70] M. L. Laursen, M. A. Samuel, and A. Sen, *Radiation Zeros and a Test for the g Value of the τ Lepton*, *Phys. Rev. D* **29** (1984) 2652–2654. [Erratum: *Phys.Rev.D* 56, 3155 (1997)].
- [71] I. Rodriguez and O. A. Sampayo, *Tau anomalous couplings and radiation zeros in the $e^+ e^- \rightarrow \tau \text{ anti-}\tau \gamma$ process*, [[hep-ph/0312316](#)].
- [72] M. Fael, L. Mercolli, and M. Passera, *Towards a determination of the tau lepton dipole moments*, *Nucl. Phys. B Proc. Suppl.* **253-255** (2014) 103–106, [[arXiv:1301.5302](#)].
- [73] J. Aebischer, W. Dekens, E. E. Jenkins, A. V. Manohar, D. Sengupta, and P. Stoffer, *Effective field theory interpretation of lepton magnetic and electric dipole moments*, *JHEP* **07** (2021) 107, [[arXiv:2102.08954](#)].
- [74] T. Hahn and M. Perez-Victoria, *Automatized one loop calculations in four-dimensions and D-dimensions*, *Comput. Phys. Commun.* **118** (1999) 153–165, [[hep-ph/9807565](#)].
- [75] T. Hahn, *Generating Feynman diagrams and amplitudes with FeynArts 3*, *Comput. Phys. Commun.* **140** (2001) 418–431, [[hep-ph/0012260](#)].
- [76] S. Banerjee, A. Y. Korchin, and Z. Was, *Spin correlations in τ -lepton pair production due to anomalous magnetic and electric dipole moments*, *Phys. Rev. D* **106** (2022), no. 11 113010, [[arXiv:2209.06047](#)].
- [77] F. Maltoni, C. Severi, S. Tentori, and E. Vryonidou, *Quantum tops at circular lepton colliders*, [[arXiv:2404.08049](#)].
- [78] M. Fabbrichesi and L. Marzola, *Quantum tomography with τ leptons at the FCC-ee*, [[arXiv:2405.09201](#)].
- [79] A. Elagin, P. Murat, A. Pranko, and A. Safonov, *A New Mass Reconstruction Technique for Resonances Decaying to di-tau*, *Nucl. Instrum. Meth. A* **654** (2011) 481–489, [[arXiv:1012.4686](#)].
- [80] **CMS** Collaboration, *Measurement of the tau lepton polarization in Z boson decays*, .

- [81] L. Bianchini, B. Calpas, J. Conway, A. Fowlie, L. Marzola, C. Veelken, and L. Perrini, *Reconstruction of the Higgs mass in events with Higgs bosons decaying into a pair of τ leptons using matrix element techniques*, *Nucl. Instrum. Meth. A* **862** (2017) 54–84, [[arXiv:1603.05910](#)].
- [82] P. Bärtschi, C. Galloni, C. Lange, and B. Kilminster, *Reconstruction of τ lepton pair invariant mass using an artificial neural network*, *Nucl. Instrum. Meth. A* **929** (2019) 29–33, [[arXiv:1904.04924](#)].
- [83] N. Tamir, I. Bessudo, B. Chen, H. Raiko, and L. Barak, *Neural networks for boosted di- τ identification*, *JINST* **19** (2024), no. 07 P07004, [[arXiv:2312.08276](#)].
- [84] L. Tani, N.-N. Seeba, H. Vanaveski, J. Pata, and T. Lange, *A unified machine learning approach for reconstructing hadronically decaying tau leptons*, [arXiv:2407.06788](#).
- [85] A. Y. Korchin, E. Richter-Was, Y. Volkotrub, and Z. Was, *τ -lepton pair spin in proton-proton LHC collisions for anomalous dipole moments*, [arXiv:2407.17282](#).
- [86] A. Cervera-Liarta, J. I. Latorre, J. Rojo, and L. Rottoli, *Maximal Entanglement in High Energy Physics*, *SciPost Phys.* **3** (2017), no. 5 036, [[arXiv:1703.02989](#)].
- [87] S. R. Beane, D. B. Kaplan, N. Klco, and M. J. Savage, *Entanglement Suppression and Emergent Symmetries of Strong Interactions*, *Phys. Rev. Lett.* **122** (2019), no. 10 102001, [[arXiv:1812.03138](#)].
- [88] I. Low and T. Mehen, *Symmetry from entanglement suppression*, *Phys. Rev. D* **104** (2021), no. 7 074014, [[arXiv:2104.10835](#)].
- [89] Q. Liu, I. Low, and T. Mehen, *Minimal entanglement and emergent symmetries in low-energy QCD*, *Phys. Rev. C* **107** (2023), no. 2 025204, [[arXiv:2210.12085](#)].
- [90] M. Carena, I. Low, C. E. M. Wagner, and M.-L. Xiao, *Entanglement suppression, enhanced symmetry, and a standard-model-like Higgs boson*, *Phys. Rev. D* **109** (2024), no. 5 L051901, [[arXiv:2307.08112](#)].